OCCASION

This publication has been made available to the public on the occasion of the 50th anniversary of the United Nations Industrial Development Organisation.

DISCLAIMER

FAIR USE POLICY

CONTACT

Please contact publications@unido.org for further information concerning UNIDO publications.

For more information about UNIDO, please visit us at www.unido.org

UNITED NATIONS INDUSTRIAL DEVELOPMENT ORGANIZATION
Vienna International Centre, P.O. Box 300, 1400 Vienna, Austria
Tel: (+43-1) 26026-0 · www.unido.org · unido@unido.org

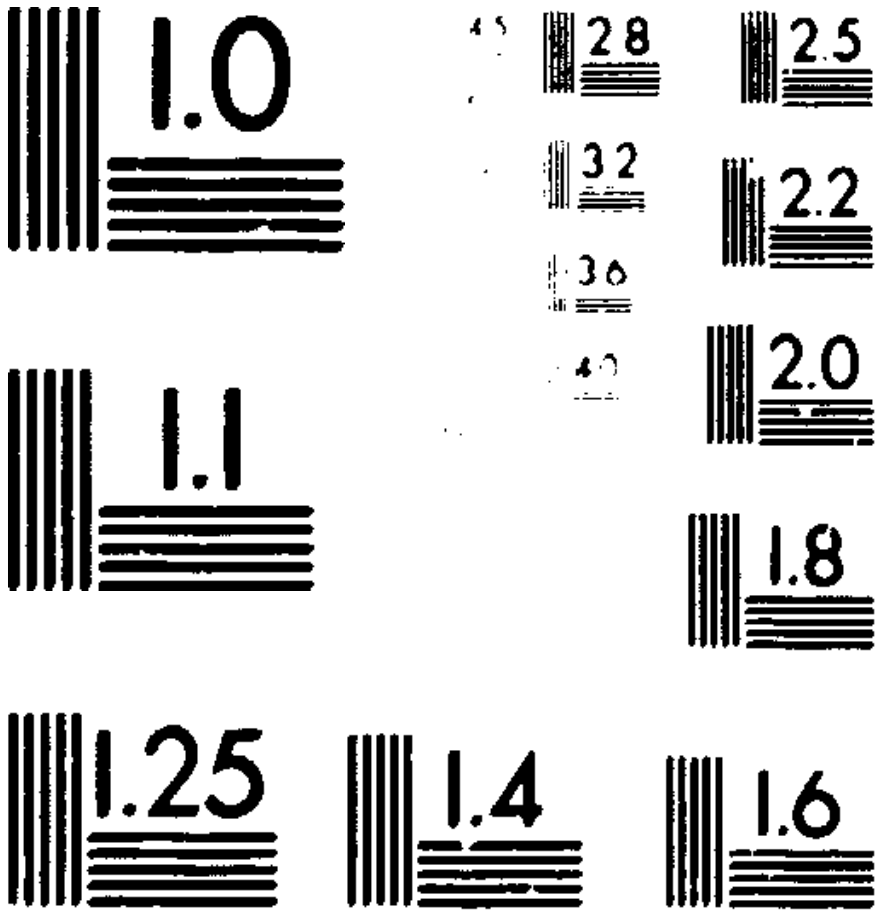

UNITED NATIONS NATIONS UNIES

UNITED NATIONS INDUSTRIAL DEVELOPMENT ORGANIZATION

14158

PHYSICAL CHEMISTRY AND PRACTICE OF ALUMINIUM ELECTROLYSIS

J. Horvath

ALUTERV - FKI

BUDAPEST

1984

UNITED NATIONS

INDUSTRIAL DEVELOPMENT ORGANIZATION

PHYSICAL CHEMISTRY AND PRACTICE OF ALUMINIUM ELECTROLYSIS

Edited by

Dr.J. HORVÁTH

Co-authors:

Dr.F. Mosóczy

Mr.G. Szina

Mr.L. Tikász

ALUTERV-FKI

BUDAPEST

1984

ACKNOWLEDGEMENT

I would like to express my thanks to Dr.János Zámbó managing director of ALUTERV-FKI and Mr. G.Szentgyörgyi deputy director for making possible to prepare this study.

I am very glad to have co-operated with my co-authors who elaborated their special topics and looked after the whole study: Dr. F. Mosóczi (anode consumption); G. Szina (energy balance); L. Tikász (cell voltage and measuring methods).

I am grateful for the precious advice of Dr.K.Solymár, Dr.P.Gadó and Dr.D.Bulkai.

Special thank is due to Mr. J.Ifjú for his friendly but firm hand.

I am thankful to Mrs. Marta Benkő (drawings) and Mrs. E.Fehér (typing).

Budapest, August, 1984

Dr. János Horváth

CONTENT

Figures	F-1
Tables	T-1
Summary	S-1
Introduction	1

		Page
1.	STRUCTURE AND PROPERTIES OF THE BATH FOR ALUMINIUM PRODUCTION	1
	1.1 Development of structural models for electrolyte	1
	1.2 Physico-chemical methods for determination of thermodynamical function in cryolite-alumina melts	2
	1.3 Physico-chemical properties of the electrolyte	7
2.	ELECTRODE REACTIONS ON ALUMINIUM AND CARBON IN CRYOLITE-ALUMINA MELTS	11
	2.1 Electrodes for use in cryolite-alumina melts	11
	2.2 Galvanic cells and reference electrode for electro chemical measuring	11
	2.3 Anode process, anodic overvoltage, anode effect	16
	2.4 Cathode reaction, role of sodium in the cathode process	27
	2.5 Anode consumption, aspects of anode performance	29
3.	CURRENT EFFICIENCY AND BACK REACTION	34
	3.1 Interraction between aluminium and the electrolyte	34

Page

3.2 Test methods for the determination of aluminium solubility 35

3.3 Reaction between CO_2-CO and dissolved metal 39

3.4 Aluminium reduction cell variables and operations in relation to current efficiency 53

4. SOLUTION PROCESSES AND TRANSPORT PROPERTIES IN THE ELECTROLYTE 65

4.1 Alumina dissolution 65

4.2 Measuring methods on alumina dissolution 67

4.3 Sludge formation 70

4.4 Kinetical aspects of alumina dissolution and crust formation 74

4.5 Formation of aluminium carbide 79

5. CELL VOLTAGE AND ENERGY BALANCE ON ALUMINIUM REDUCTION CELLS 84

5.1 Theoretical energy requirement of Hall-Heroult process 84

5.2 Cell voltage components 86

5.3 Energy efficiency 90

6. FUTURE TRENDS, RESEARCH AND DEVELOPING PROGRAMS IN PROCESS METALLURGY OF ALUMINIUM 92

REFERENCES

FIGURES

Fig.1. The anion fraction of the cryolite as a function of molar ratio

Fig.2. Species in the cryolite-alumina melts

Fig.3. The specific conductivity of Na_3AlF_6-Al_2O_3 mixtures

Fig.4. Vapour pressures in the system NaF-AlF_3-Al at 1028 ^oC

Fig.5. Aluminium electrode

Fig.6. The anode-potential-current density relationship on grafite

Fig.7. Anode potential v.s. time diagram

Fig.8. The cathodic overvoltage on aluminium in cryolite-alumina melts at various temperature

Fig.9. Mass transfer in the cathodic layer

Fig.10. Anode consumption v.s. current density

Fig.11. The anode consumption - calcination temperature relationship

Fig.12. The effect of pitch content of the different properties of anode paste

Fig.13. Vapour pressures in presence of aluminium

Fig.14. Polarization curves on Pt electrode in the cases of pure aluminium and aluminium-copper alloys

Fig.15. Rate of reoxidation as function of cryolite ratio

Fig.16. Rate of reoxidation reaction as a function of temperature in presence of CO_2

Fig.17. Effect of CO_2 gas induced on the rate of re-oxidation process

Fig.18. Rate of formation of CO(rf_{CO}) as a function of temperature

Fig.19. Arrhenius plot of the rf_{CO}

Fig.20. The effect of the mechanical stirrer on the rf_{CO}

Fig.21. The rf_{CO} and i_c as a function of the speed of rotation of the stirrer

Fig.22. The rf_{CO} as function of speed of rotation of the stirrer

Fig.23. The limiting current i_c as function of depth immerson of Pt electrode

Fig.24. The rf_{CO} as a function of distance of the bubbling tube above the metal surface

Fig. 25. Proposed concentration profile of dissolved metal

Fig.26. Determination of aluminium inventory in operating cell

Fig.27. Current efficiency as a function of bath temperature in laboratory cells

Fig.28. Current efficiency versus temperature in commercial cells

Fig.29. The influence of cryolite ratio on the current efficiency for laboratory cells

Fig.30. The influence of cryolite ratio on the current efficiency in commercial cells

Fig.31. Current efficiency v.s. alumina content in laboratory cells

Fig.32. The influence of alumina on the current efficiency in industrial cells.

Fig.33. The influence of interelectrode distance on current efficiency for laboratory cells

Fig.34. The influence of interelectrode distance on current efficiency for commercial cells

Fig.35. Calibration curves for determination of the alumina and sludge dissolution

Fig.36. Changes of rf_{CO} by addition of excess alumina to cryolite alumina melts

Fig.37. Increase in alumina content in cryolite melt in contact with sludge

Fig.38. Effect of mechanical stirring on rf_{CO} as a function of the amount of excess alumina added

Fig.39. Dissolution curves at normal and crustlike aggregation

Fig.40. Dissolution curves at different temperature

Fig.41. Aluminiumcarbide formation v.s. reaction time

Fig.42. The carbide formation v.s. the alumina content of cryolite melt

Fig.43. Cell voltage components and energy consumption

TABLES

Table 1. Anode consumption at prebaked and Söderberg electrode

Table 2. The free energy changing for reaction between aluminium and electrolyte

Table 3. Reactions between gas and dissolved metal

Table 4. The kinetic parameters of alumina dissolution

Table 5. Physical properties of studied aluminas

SUMMARY

The main target to give an up-to date comprehensive overview of the state-of-the-art in physical-chemistry background of aluminium production. The theoretical background will be given, but practical aspects will be emphasized through the sharing of operational experience. The objective of this study is to give physical-chemistry knowledges in the proper understanding of the process.

Proper understanding of process is a basis for inproving of aluminium production. A more detailed melt structure study explains the bath evaporation.

Similarly a more detailed understanding of the electrode processes is necessary for having a good model for cell operation and control. A proper heat balance of the cell needs proper understanding of fundamental thermodynamic reactions involved. The bath chemistry, composition will be determinedthe operating temperature of the cell.

Our aim is to give help for achievement a more efficient operation of aluminium smelters through a better understanding of Hall-Heroult process.

INTRODUCTION

The bath composition in aluminium electrolysis cell varies considerably. Because of the Chapter 1. we have published structural model of the bath and physical-chemistry properties of electrolyte.

Several attempts have been made during the last years to improve the current efficiency. This has been possible because of increased understanding of chemical and electrochemical processes that occur in the bath. (Chapter 2.3)

The electrochemical problems discussed are of great importance, anode cathode overvoltage, and particulary anode effect.

The chemical reaction between the dissolved metal and CO_2 is the most important reason for the lowering in current efficiency. We interpret the theoretical background of reoxidation reaction.

In order to minimize the sludge formation the rate of alumina dissolution should be high. Because of we study the kinetics of alumina dissolution in the bath. (Chapter 4.)

On the base of electrochemical measurements will be studied the cell voltage and energy balance of the cell. (Chapter 5.)

1. STRUCTURE AND PROPERTIES OF THE BATH FOR ALUMINIUM PRODUCTION

1.1. Development of structural models for electrolyte

In the electrolytic production of aluminium, the electrolyte of a solution of about 3 to 8 weight per cent aluminium oxide in molten cryolite. To understand the chemistry of the electrolytic process, a knowledge of the constitution of the solvent and the interraction of the solvent with the solute is essential. There are two stages in the development of structural models for the electrolyte used in aluminium production. The first is connected with the structural entities in molten cryolite. The second is to predict whether defined ions are formed by the dissolution in molten cryolite.

The two component system sodium-fluoride-aluminium has been investigated for determination of cryolite structure in molten phase.

In the phase diagram high peak at the compound cryolite indicates that this compound is quite stable. This is also supported by the large negative value of the heat of formation of cryolite.

It would be expected, that AlF_6^{3-} ions are quite stable in liquid state. This is indicated by calculations of the liquidus line. However, the curveture of the cryolite peak in the phase diagram indicate a slight dissociation of complex anion.

The comparing the experimentally established liquidus curve of cryolite in the $NaF-AlF_3$ system with the theoretical one, it is found, that cryolite dissociate

$$Na_3\,AlF_6 \longrightarrow 3Na^+ + AlF_6^{3-} \qquad (1.1)$$

$$AlF_6^{3-} \rightleftharpoons AlF_4^- + 2F^- \qquad (1.2)$$

The anion fraction the cryolite as a function of molar ratio is shown in Fig.1.

When aluminium oxide is dissolved in molten cryolite O^{2-} ions and additional Al^{3+} ions are introduced into the system. Aluminium ions are already present in the system as complex ion. The added O^{2-} ions are quite similar in size to the F^--ion and can substitute for these structurally. Hence it is a fair assumption that the O^{2-} ions introduced into molten cryolite will occupy essentially the same type of site as the F^- ions, and that they will be statistically distributed around Al^{3+} ions in the melt as $AlOF_x^{1-x}$ complex ions, where one would expect strong bounds between the Al^{3+} and O^{2-} ions. The mixture can then be treated as consisting of Na^+ ions and $AlOF_x^{1-x}$ and AlF_y^{3-y} complex ions. The experimental data indicate that association of the $AlOF_x^{1-x}$ complex takes place.

Based an activity data in $NaF-AlF_3$ melts saturated with Al_2O_3 it is indicated, that presence of two species in the $Na_3AlF_6-Al_2O_3$ melts:

$Al_2OF_6^{2-}$ at low alumina concentration and $Al_2O_2F_4^{2-}$ at high concentrations of alumina, while the oxyfluoride anions, $Al_2O_2F_6^{4-}$ and $Al_2OF_{10}^{6-}$ might only be present in small amounts at the cryolite composition.

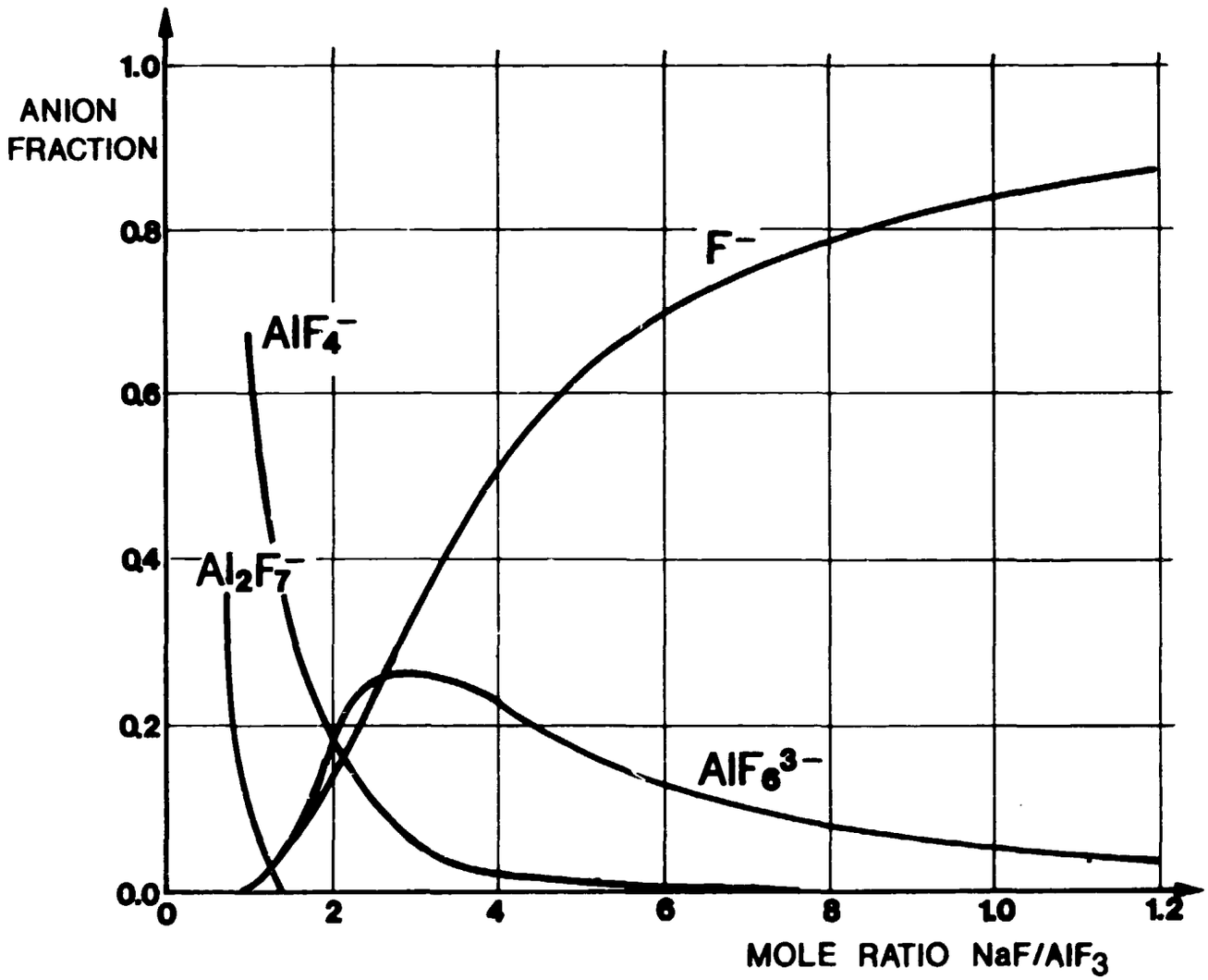
1.0
ANION
FRACTION
0.8
0.6
0.4
0.2
0.0
0
2
4
6
8
1.0
1.2
MOLE RATIO NaF/AlF3
F⁻
AlF4⁻
Al2F7⁻
AlF6³⁻

Fig.1.

On the base of measurements the proposed mechanism of alumina solution:

$$Al_2O_3 + 4AlF_6^{3-} \longrightarrow 3Al_2OF_6^{2-} + 6F^- \qquad (1.3)$$

at low alumina concentration

and

$$2Al_2O_3 + 2AlF_6^{3-} \longrightarrow 3\ Al_2O_2F_4^{2-} \qquad (1.4)$$

In the cryolite-alumina melts the following species are present.

Na^+, F^-, AlF_6^{3-}, AlF_4^- $Al_2OF_6^{2-}$, $Al_2O_2F_4^{2-}$, $Al_2O_2F_6^{4-}$ $Al_2OF_{10}^{6-}$

This is indicated in Fig.2.

1.2. Physico-chemical methods for determination of thermodynamical function in cryolite-alumina melts

Interaction between the mixture is interpreted by activity measuring. Experimental methods for activity determination is cryoscopy, vapour pressure measuring, solubility measurement, calorimetry and concentration cell.

Cryoscopy:

Basis of the cryoscopic method is that the freezing point depression of a solvent caused by small amounts of solute, depends on the solvent used.

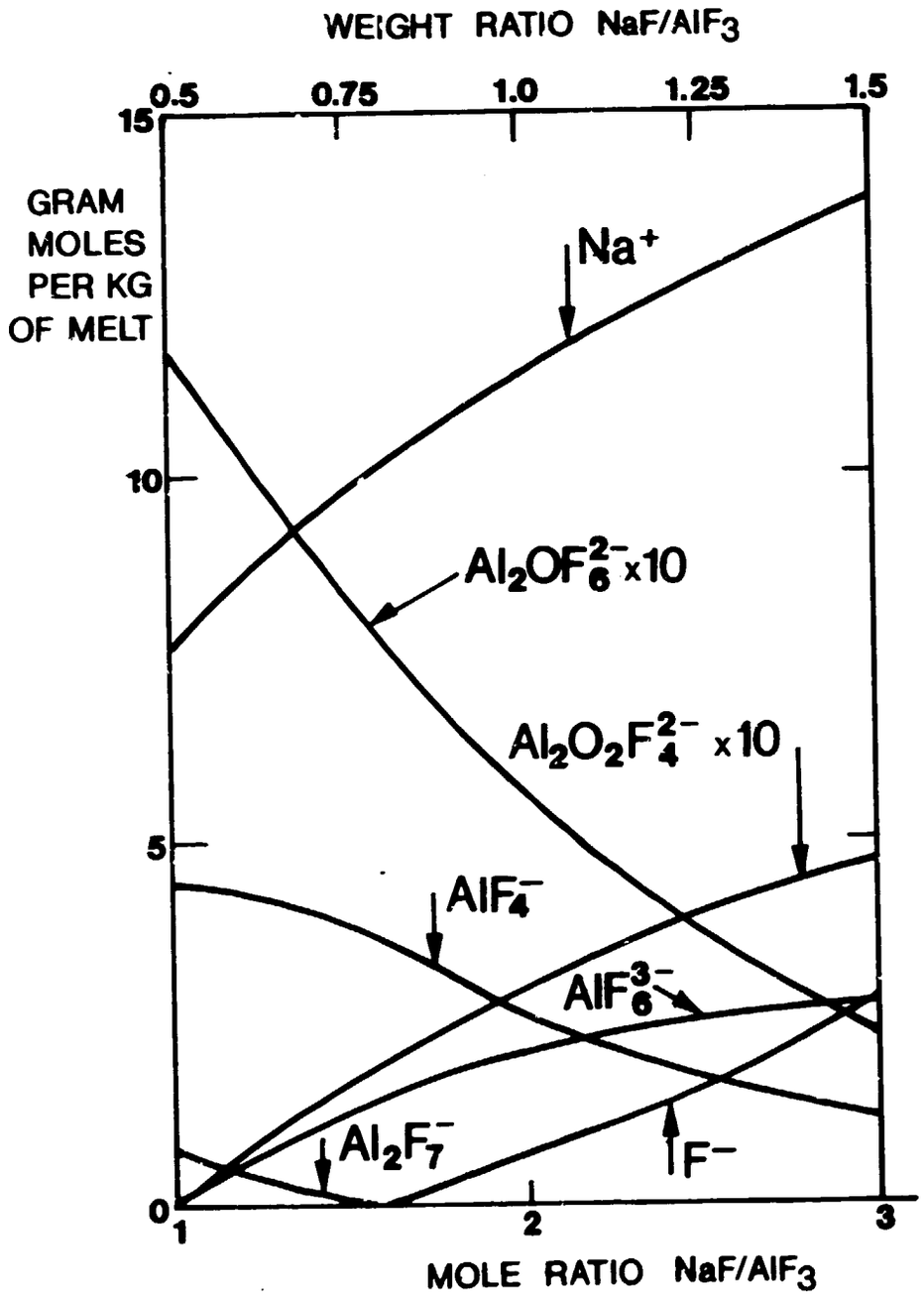

Fig.2. (See Ref. 2.)

The $\ln a_i = - \frac{\Delta H_f}{R} \left(\frac{1}{T} - \frac{1}{T_o} \right)$ express (1.5)

equation.

The relationship between activity and freezing point depression, assuming that ΔH_t is independent of the temperature.

Vapour pressure measurements:

The vapour pressure of a component is convenient measure of its activity. The activity may be calculated from vapour pressure measurements by use of the simple equation.

In the $a_A = \frac{p_a}{p_A^o}$ equation (1.4) p is the vapour pressure of the component A and the superscript O denotes the standard state.

Solubility measurements:

The activity in binary salt system may be determined from metal-molten salt equilibria.

Calorimetry:

Calorimetric measurements can be used to determine the thermochemical data. On the base of relationship between entalpies of mixing, binary interaction parameters and mol fractions can be used to calculate activities.

Concentration cell:

Measurements of the electromotive force of concentration cell Al(A, B,)Y /diaphragm/ (A,B),, Y/A may be determined ΔE value.

From $$\Delta E = - \frac{\Delta G}{nF} = - \frac{RT}{nF} \ln \frac{a_{AY(I)}}{a_{Yy(II)}} \quad \frac{a_{BY(II)}}{a_{BY(I;}} \qquad (1.5)$$

equation (1.5) is given the activity value.

1.3. Physico-chemical properties of the electrolyte

In the aluminium electrolysis very important properties are the followings:

- liquid temperature of electrolyte
- electrical conductivity
- vapour pressure
- density
- viscosity
- surface tension

When the electrolyte drops below the liquidus temperature, a precipitate forms. The ideal operating temperature will be sufficiently above the liquidus to provide the heat of solution for alumina additions without falling below the liquidus temperature.

High electrical conductivity is obvious advantage. This information is important in obtaining a better understanding of the mechanism of transport processes. High conductivity produces a lower cell voltage and consequently less generation of heat.

The electrical conductivity of cryolite-alumina melts has been measured and there is divergence among the reported value. The specific conductivity of cryolite and cryolite-alumina melts is shown in Fig.3.

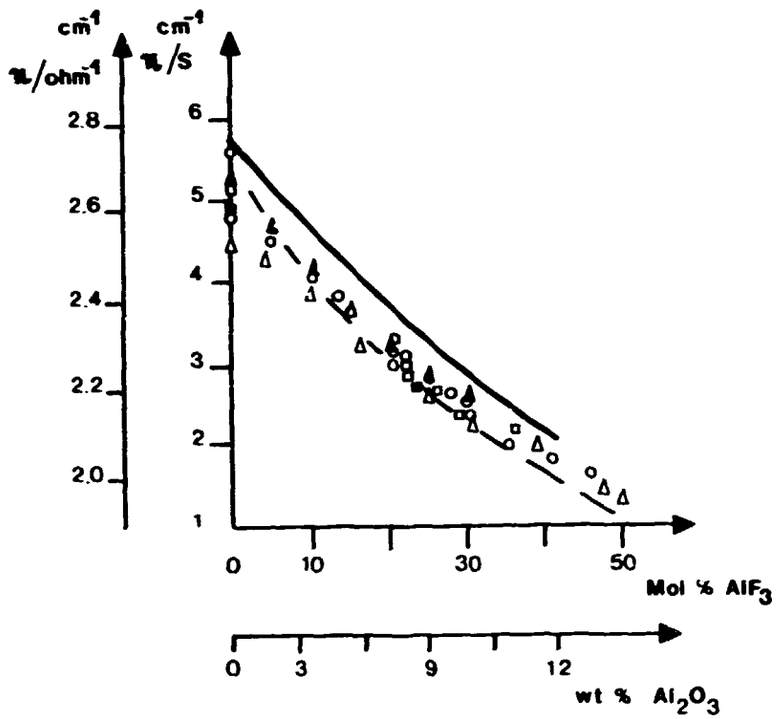

It may be assumed, that the decrease in conductivity with increasing alumina concentration is caused by decrease in the concentration of Na^+ ions which countributes considerably to the conductivity of cryolite melts.

Vapour pressures was measured above NaF + AlF_3 - Al mixtures. The vapour pressure over the melt in absence of aluminium and in presence of aluminium is difference. In Fig.4. is shown the vapour pressure.

Density of electrolyte is important from a practical standpoint because, the difference in density between the melt and molten aluminium is small.

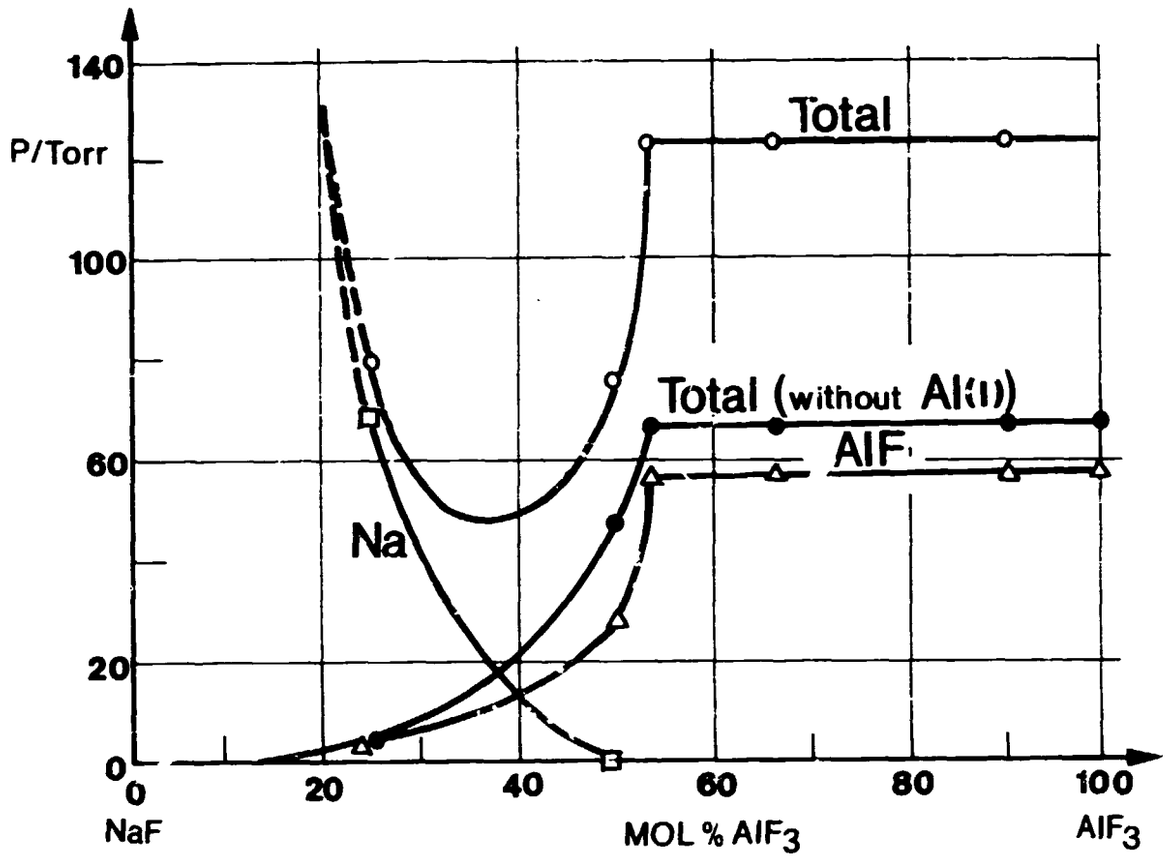

VAPOUR PRESSURES IN THE SYSTEM $NaF-AlF_3-Al$ at 1028°C

Open circles: Total vapour pressure with Al [1] present
Filled circles: Total vapour pressure without Al [1] present
Squares : Partial vapour pressure of Na [g]
Triangles : Partial vapour pressure of AlF [g]

Fig.4. (See Ref.2.)

The difference in density between bath and metal affects the separation of the metal deposited from the bath and also the rate of dissolution of aluminium in the electrolyte. The density difference is close to 0.2 g/cm^3, becomes too small, a turbulent metal pad would increase heavily the motion of dissolved metal. So, the current efficiency is decreased.
It is noted, that the density of industrial bath may be influenced by suspended carbon skimming from anode paste.

Viscosity is one of parameters governing the hidrodynamic processes in the cell, like convection, (bath and metal velocities) and sedimentation of alumina particles. The high viscosity reduces the diffusion and thus the transport of dissolved metal to the anode. TØrklep and Øye reported, that with increasing of AlF_3 in the bath will reduce the viscosity. (1)

The interfacial tension between metal and bath is defined as the difference between the surface tensions of the metal and bath. The high value of tension interfacial is beneficial in order to reduce the transport of metal through the interface.
The interfacial tension between the electrolyte and carbon influences the penetration of electrolyte into the porous of the carbon and the separation of carbon particles from the electrolyte.

2. ELECTRODE REACTIONS ON ALUMINIUM AND CARBON IN CRYOLITE-ALUMINA MELTS

The chemical and electrochemical reactions taking place at near anode and cathode of a Hall-Heroult cells are of great practical and theoretical importance. Although not fully understood, in spite of extensive research, enough is known to farm a reasonably consistent picture. Diffusion, convective mass transport, and electronic transport all play important roles in the electrode processes.

2.1. Electrodes for use in cryolite-alumina melts

While the carbon lining of the cell is often referred to as cathode, the true cathode is the molten aluminium that rests on it. Generally, the sides of the cell cavity are covered with frozen electrolyte that often contains undissolved alumina. This frozen ledge thermally and electrically insulates the sidewalls and prevents their acting of cathodes. The anodes, either prebaked carbon blocks or continuous self-baking Söderberg electrodes, are suspended in the electrolyte.

2.2. Galvanic cells and reference electrode for electrochemical measuring

Galvanic cells are used to study chemical equilibria and to derive thermodynamic data. In cryolite-alumina melt the method give a possibility for the determination of the activity of reacting species. However, the available electrodes do not usually show the high degree of reproducibility required for activity measurements.

In electrochemical kinetic studies where current is passed through cell, a third electrode which does not carry current, the reference electrode is.

The difference in potential is measured between the reference and working electrode during study.
The various type of electrodes used in cryolite system are listed below:

1.) Gas electrodes
   a) flushed with gas (Pt_2O_2; Pt, CO_2; C, O_2; C, CO; C, (CO_2 + CO)
   b) without flushing (C)

2.) Oxide electrodes (Fe_2O_3; Fe_3O_4; Cr_2O_3; SnO_2)

3.) Metal electrodes
   a) aluminium
   b) alloys of aluminium and sodium
      - solid alloys (Fe-Al, Pt-Al)
      - liquid alloys (Pb-Na)
   c) metals other than aluminium and sodium (Pt, W)

4.) Electrode with liquid junction.

Gas electrodes:

The cell $Al(Na_3AlF_6 + Al_2O_3)PtO_2$ with the $2Al + \frac{3}{2} O_2 = Al_2O_3$ cell reaction show that given result agreed with the theoretical decomposition potentials based on thermodynamic data for a saturated solution of alumina in cryolite. Any deviation from reversible potential can be attributed to the Pt, O_2 electrode.

For the C, CO_2 reference electrode the standard emf of the cell, $Al(Na_3AlF_6+Al_2O_3)CO_2$ C, with the assumed cell reaction

$2Al + \frac{3}{2} CO_2 = Al_2O_3 + \frac{3}{2} CO$ is 1.169 V at 1000 ^oC for a saturated solution of alumina in cryolite.

In this case is necessary to flush continuous the CO_2, in order to maintain a stable potential. Because of $CO_2 + C = CO$ reaction, may be difficult to obtain pure CO_2 at the melt-carbon-gas interface.

To avoid this problem the C CO electrode may be considered. It is found, that C/CO electrode to be more stable, with reproducibility of $\pm$ 3-5 mV.

2. Oxide electrodes

Behaviour of electrodes of metal oxide is characterised with the following type of cells

$W(Na_3AlF_6 + Al_2O_3)\ Cr_2O_3$ inconel

$W(Na_3AlF_6 - Al_2O_3)\ Fe_2O_3$, Fe

$W(Na_3AlF_6 + Al_2O_3)\ SnO_2$, Pt.

For the cell

$Al(Na_3AlF_6 + Al_2O_3)\ Cr_2O_3$ the corresponding standard potential is 1.4 V. Relationship between activity and molar fraction of alumina is unreasonable.

For the cell $Al(Na_3AlF_6 + Al_2O_3)\ SnO_2/Pt$ is given reasanable relationship between activity and molar fraction of alumina.

The cell have to be kept under protective atmosphere. A plot of the potential versus the logarithm of the molar fraction of alumina give a straight line. Extrapolation to pure alumina give a value of 1.36 V at 1300 ^{o}K, in agreement with the theoretical value for the reaction:

$$2Al + \frac{3}{2} SnO_2 = Al_2O_3 + \frac{3}{2} Sn \qquad (2.1)$$

The slope of the curve give the relationship

$$a_{Al_2O_3} = N_{Al_2O_3}^{3} \qquad (2.2)$$

which is reasonable if a complete dissociation of alumina is considered. The SnO_2 electrode is clained to be chemically stable under oxidizing conditions and the emf is stable within $\pm$ 5 mV. (7)

3. Metal electrodes

Aluminium electrode is shown in Fig.5.

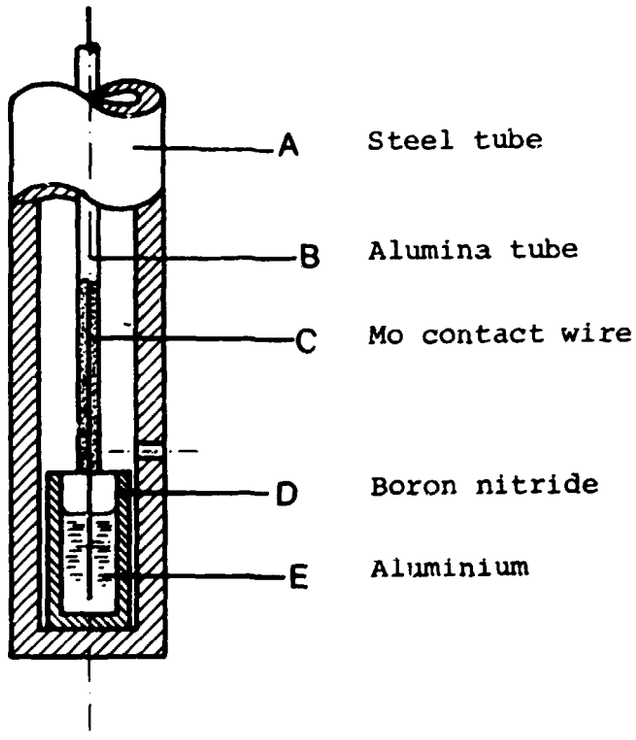

Most workers have found that the aluminium electrode shows satisfactory stability as a reference electrode. In general, the stability of aluminium electrode is within 3-5 mV is slightly better than for C, CO_2 electrode.

Solid aluminium alloys is used especially for measurements in industrial cells. Solid electrodes may be prefferred in the form of a rod consisting of an aluminium alloy. Provided that the other component is more noble than aluminium, such an electrode will behave as an aluminium electrode although the aluminium activity will be less.

Liquid aluminium alloys do not affer advantages as reference electrodes compared to pure aluminium.

Sodium electrodes, Pb-Na alloys have been used for equilibrium and activity measurements.

Electrodes with liquid junction:

In concentration cell studies the two half cells must be connected by an ionic conductor, i.e, some kind of a diaphragm or salt bridge. Contact between the two melts can be achieved through a small hole, but diaphragm materials are used, too, So, sintered Al_2O_3, MgO, ZrO_2-CaO and BN.
In the case of sintered oxides and boron nitride the melt will soak through the diaphragm, whereas CaO-stabilized zirconia can act as a solid oxigen ion conductor.

As a concusion it may be stated there is no electrode which is universally applicable as a reference electrode in cryolite melts.

As our opinions the C CO, SnO_2 electrodes seems to be the rest choice, which verified for determination of alumina activity. (6,7)

2.3. Anode process, anodic overvoltage, anode effect

Alumina dissociates by dissolution in cryolite. It is believed, the $Al_2OF_6^{2-}$ and $Al_2O_2F_4^{2-}$ oxigen containing complex ion generates.

This suggests that the anode reaction is:

$$2Al_2O_2F_4^{2-} + C \longrightarrow CO_2 + 2Al_2OF_4 + 4e^- \qquad (2.3)$$

$$Al_2OF_4 + 2Al_2OF_6^{2-} = Al_2O_2F_4^{2-} + 4AlF_3 \qquad (2.4)$$

This later reaction restore the equilibrium between $Al_2OF_4^{2} - Al_2OF_6^{2-}$

Using linear potential sweep method for study of anodic process on polarization curve indicates different peaks.
On grafite electrode the anode potential-current relationship indicate Fig.6. (11)

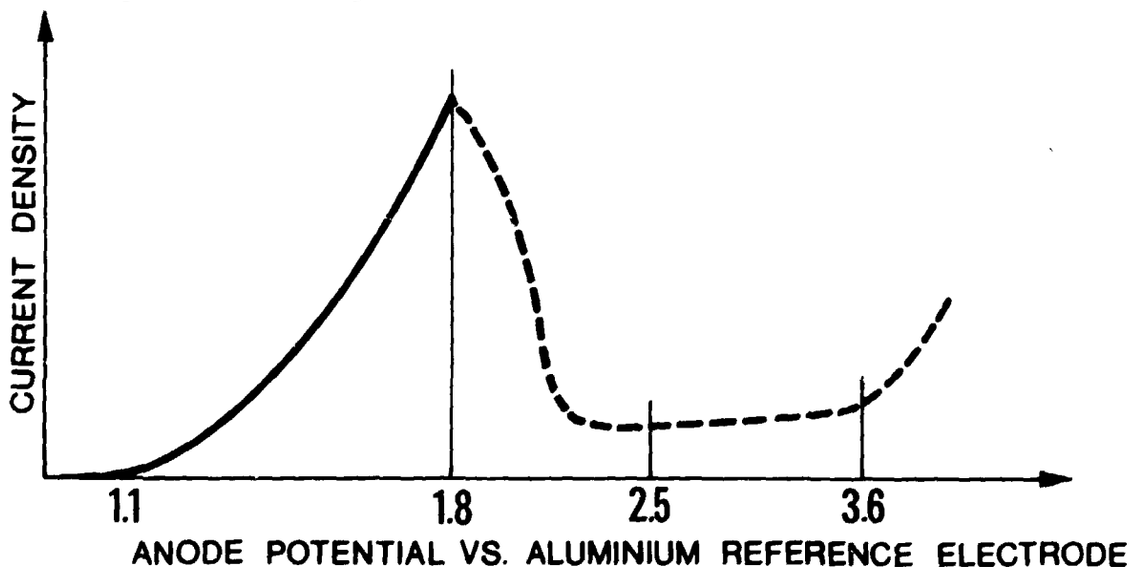

The voltamograms of anodic process on grafite found current-breaking at 1.1; 1.8; 2.5 and 3.6 Volts versus an aluminium electrode. Comparing these patentials with standard thermodynamic potentials for a number of reaction is given:

$$Al_2O_3 + 3C = 3CO + 2Al \qquad E^o = 1.02\ V \qquad (2.5)$$

$$2Al_2O_3 + 3C = 3CO_2 + 4Al \qquad E^o = 1.16\ V \qquad (2.6)$$

$$2Na_3AlF_6 + Al_2O_3 + 3C = COF_2 + 6NaF + 4Al$$
$$E^o = 1.8\ V \qquad (2.7)$$

$$4Na_3AlF_6 + 3c = 3CF_4 + 12NaF + 4Al$$
$$E^o = 2.55\ V \qquad (2.8)$$

$$2Na_3AlF_6 = 3F_2 + 6NaF + 2A$$
$$E^o = 4.41\ V \qquad (2.9)$$

The 1.1 V and 1.8 V peaks correlated with alumina concentration. (See ref.12.)

At 1.8 V potential the current decreasing may be explain with formation COF_2, although COF_2 has never been found in the pot gas. COF_2 quickly hydrolyse with moisture in the air to CO_2 and HF.
It is probably, that reaction of CF_4 formation is responsibile for anode effect.

The anode mechanism must explain the large displacement from termodynamic equilibrium oxigen reacting with

carbon at cell temperature should equilibriate to about 99 % CO and 1 % CO_2. Based an the volume of gas produced and net carbon consumed, however, the primary product formed at the anode is essentially all CO_2.

During current flow E_i polarization potential and the reversible cells potential is difference. Magnitude this difference means the anodic overvoltage. At industrial current density it is to be 400-600 mV.

What cause this difference and what is the rate determining step in the anode reaction?

Practically all workers who the anode mechanism, have studied established that the current-voltage behaviour follow the Tafel-law.
In this case the anode process is controlled by the slow chemical reaction or transport of oxigen carrying ion through the double layer.
An the base of extensive investigation for anode reaction was made by Thonstad. He analysed anode overvoltage using Vetter relationship for anode reaction overvoltages at normal current density and at very low current densities.(12)

$$\eta_r = \frac{RT}{npF} \ln \frac{i}{i_o} \qquad (2.10)$$

$$\eta_r = \frac{RT}{npF} \frac{i}{i_o} \qquad (2.11)$$

It is found, the reaction order is (p) = 0.57 and n = 2

This values give information about, that one oxygen atom must be involved in the rate controlling step, n can not be less then 2.

If the overvoltage is caused by slow transport of oxigen carrying ions through the double layer, when the Butler-Volmer, Erdey Gruz relationship would apply.

$$\eta_r = \frac{RT}{\alpha nF} \ln \frac{i}{i_o} \qquad (2.12)$$

at normal current densities

$$\eta_r = \frac{RT}{\alpha nF} \quad \frac{i}{i_o} \qquad (2.13)$$

at low current densities.

In this case i_o is the exchange current density and α the charge transfer coefficient. The exchange current represents the electrode reaction rate at equilibrium, where the forvard reaction equals the reverse reaction. is called the symmetry factor, a value of 0.5 represents perfect symmetry. Analysis of same data by later equation leads to a reasonable value of 0.57 for alpha.
Hence from these data alone not possible take distinquish between slow transport through the double layer and a slow chemical reaction.

To resolve the problem, Thonstad utilized an other relationship from Vetter.

$$\frac{d\ln i_o}{d\ln C} = p \qquad (2.14)$$

This gave a reaction order of p = 0.56 in excellent agreement with the reaction order from equations (2.10) and 2.11) and supports a reaction type overvoltage.

Further arguments of reaction overvoltage are:

- the primary anode product is CO_2
- the potential increase and decay is slow when is utilized non-steady-state methods
- the curves are given by impedance measurements indicates reaction overvoltage
- anode consumption depend on composition and additive.

Most of the studies fit the following proposed anode reaction. Single oxygen is discharged from $Al_2O_2F_4^{2-}$. The discharged oxygen is chemisorbed on the surface:

$$O^{2-} + xC_{(surface)} \longrightarrow C_x{}^{*}O^{-} + e^{-} \qquad (2.12)$$

$$C_x{}^{*}O^{-}{}_{(surface)} \longrightarrow C_x{}^{*}O + e \qquad (2.13)$$

Oxygen deposits an the most active sites. $C_x{}^{*}O$ surface compound is believed to be very stable. Breaking the C-C bond to form CO proceeds slowly

$$C_x{}^{*}O_{(surface)} \longrightarrow CO_{(ads)} + (x-1)C \quad (slow) \qquad (2.14)$$

The desorption of CO from the surface is probably rapid, but this has not been establised.

$$CO_{ads} \longrightarrow CO_{(gas)} \qquad (2.15)$$

Carbon sites occupied by oxygen are not easily available for further oxygen discharge. Oxygen discharge takes place on less active carbon sites requiring additional energy (overvoltage). It the all available surface is covered with C_x^*O, it is necessary, that oxygen is deposited by carbon, already bonded to oxygen.

$$C_x^*O_{(surface)} + O^{2-} = C_x^*O_2^-{}_{(surface)} + e^- \qquad (2.16)$$

$$C_x^*O_2^-{}_{(surface)} = C_xO_2{}_{(surface)} + e^- \qquad (2.17)$$

This requires still higher energy (overvoltage), accounting for the high anode overvoltage (over 0.5 V). The C-C bonds of $C_x^*O_2$ deposit easily, forming adsorbed CO_2 and new surface.

$$C_x^*O_2{}_{(surface)} = CO_2{}_{(ads)} + (x-1)C_{(surface)} \qquad (2.18)$$

adsorbed CO_2 desorbs rapidly, escaping into the bath.

The rate determining step is either

$$C_x^*O^-_{(surface)} \longrightarrow C_x^*O_{(surface)} + e^- \qquad (2.19)$$

reaction or

$$C_x^*O_2^-{}_{(surface)} \longrightarrow C_x^*O_2{}_{(surface)} + e^- \qquad (2.20)$$

reaction.

Anode overvoltage, in addition to being important in understanding the anode reaction, is of practical importance as part of the cell voltage.

Bath plant and laboratory anode overvoltage data verify validity of Tafel-line for reaction overvoltage. The reaction order p ranges from 0.5 to 0.6 for industrial carbon, varying with reactivity and porosity. The reaction limiting current density i_o ranges from 0.0039 to 0.085 A/cm^2 as alumina concentration varies from 2 to 8 wt%.

Gas bubbles generation by anode reaction increase the effective resistivity of the electrolyte around the anodes and also incrase the true overvoltage by raising the local current density in areas not covered by bubbles.

The ohmic part of the bubble effect can be measured:
- by interrupting the current
- superimposing alternating current

Haupin (8) has shown the presence of bubbles contributes between 0.09 and 0.35 V depending on the bath composition and hydrodinamics.

At low alumina concentration, diffusion overvoltage becames an important contributer to anode overvoltage. It can be calculated by the following relationship.

$$\eta_d = \frac{RT}{2F} \ln \frac{i_c}{i_c - i} \qquad (2.21)$$

where i_c is the critical or concentration limiting current density.

Thonstad determined this critical current density as function of alumina content and temperature (9)

$$i_c = [0.2+1.37(\text{wt\% } Al_2O_3)] \cdot (1\pm0.002)(T-1293) \qquad (2.22)$$

Relationship from Piontelli seems to fit industrial cell better

$$i_c = \emptyset\ [5.5+0.018(T-1323](A^{-0.1}\ [(\%Al_2O_3)^{0.5}-0.4] \qquad (2.23)$$

The symbol $\emptyset$ is a shape factor equal to one for a horizontal planar anode and equal to 1.4 for hemispherical anode. (14)

Discussion of the anode process to this point has been confined to normal operation.
When the alumina concentration in the cell is nearly depleted, a phanomenon referred to as the anode effect tales place. Whith a constant potential electric power source, the current falls to a low value. With a constant current source, the usual industrial case, the applied potential rises to 30 or more volts and the current penetrates the gas film by a multitude of small electric arcs.

In aluminium electrolysis the electrical manifestation is typical of concentration overvoltage. Anode overvoltage rises very gradually as alumina is depleted until a certain critical bulk alumina concentration.

The chemical manifestation of the anode effect in the Hall-Heroult cell is a change in anode gas composition from largely CO_2, to largely CO, with significant quantities of Cf_4 (3-20 %).

It is showed, that the onset of anode effect corresponds to the formation of fluorocarbon compounds, when the oxide ion concentration is depleted at the bath-carbon interface.

This a film type passivity is produced. The film modifies the wetting properties of the interface.

Calandra (12) points and that although continuous gas film is always present in industrial cells at anode effect, this is not a requisite. Anode effect can be produced before bubbles form by using a fast anodic sweep or a short current pulse greater than the critical current density.

Thonstad J. et al. (15) measured the critical current density and voltage at the onset of anode effect as a function of alumina concentration and gas pressure on the cell.

Evalution of CF_4 was found both before and after the onset of anode effect. It is established, that CF_4 evalution started at about 2.8 V positive to an aluminium reference electrode or about 1.6 V anode overvoltage. This value agree well with earlier mentioned results. Anode effect occured at 3.5 V and 0.11 A/cm^2 in alumina-free purified cryolite.

In summary, the anode effect is produced as alumina is depleted and anode overvoltage increasis. There is an increase in surface tension of the melt with decreasing alumina concentration. This, coupled with the electrocapillary effect resulting from the higher anode

voltage, reduces wetting of anode by the electrolyte and gas bubbles to become adherent, grow larger. Large bubbles increase to local current density an the anode, further increasing overvoltage at between 1.1-1.2 volts anode overpotential, fluorine carbon compounds are produced at the anode surface faster than they can decompose. Fluorocarbon compounds have low surface energy and promot dewetting and growth of a gas film on the anode.

In constant current applications 30 or more volts develop across this gas film. The electrolysis of fluorine maintains the dewetted surface. Even if the alumina concentration is restored, the cell will remaine on anode effect until either the current is interrupted for 10 ms or more, as by splashing aluminium to short circuit the cell and allow the gas film to collapse, or new anode area not contaminated with fluorine is exposed, as by lowering the anodes.

In industrial cells the AE normally arises at alumina contents between 0.5- and 2.2 wt% Al_2O_3 with value between 1 and 2 wt% appearing most frequently.

The cells which are a good condition and run at a low temperature tend to have the AE at low contents 0.5-1 wt% Al_2O_3. Troubled cells, may undergo the AE at alumina contents for above 2 wt% Al_2O_3. Measurement of the anode potential by means of reference electrode and by extrapolation of current-voltage curve at I = 0 show the increase is due to increasing in anodic overvoltage with decreasing alumina content. The duration and the magnitude of potential increase depend on alumina content at which AE occurs. If the alumina content goes down to

0.5 % Al_2O_3, the increase may start 2-3 hours in advance, while it may be last only 15 minutes if the AE occurs at around 2 wt% Al_2O_3.

Anode potential v.s. time diagram is shown in Fig.7. (See. Ref. 15, 16, 17)

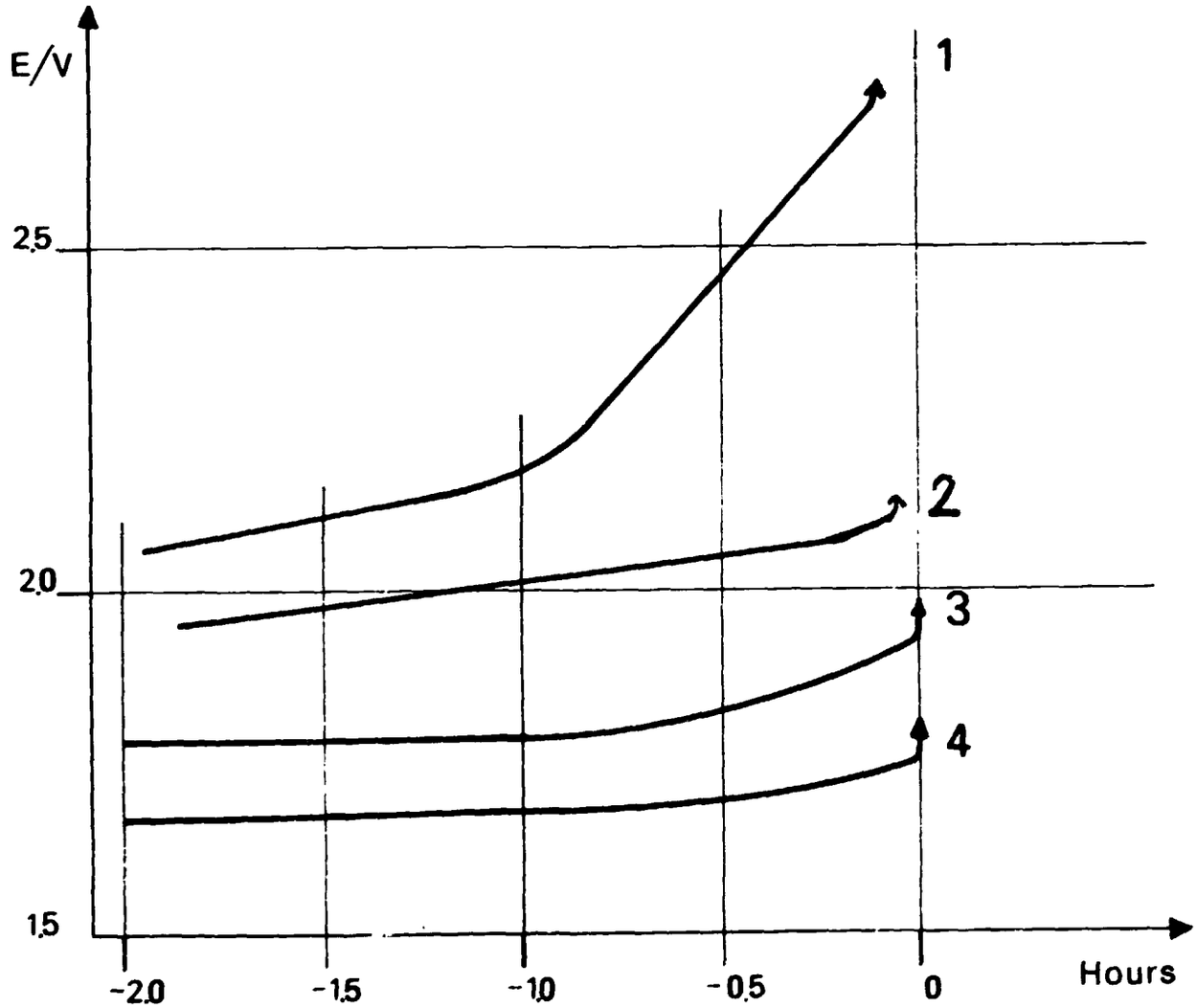

Fig. 7.

2.4. Cathode reaction, role of sodium in the cathode Process

The cathode process have less importance than the anode process. The reaction occuring at the cathode have been considered to be simple. The cathode reactions are important because they may be connected with formation of dissolved metal and thereby with current efficiency.

The cathodic overvoltage an aluminium in cryolite alumina melts at various temperature is shown in Fig.8. (See. Ref. 18)

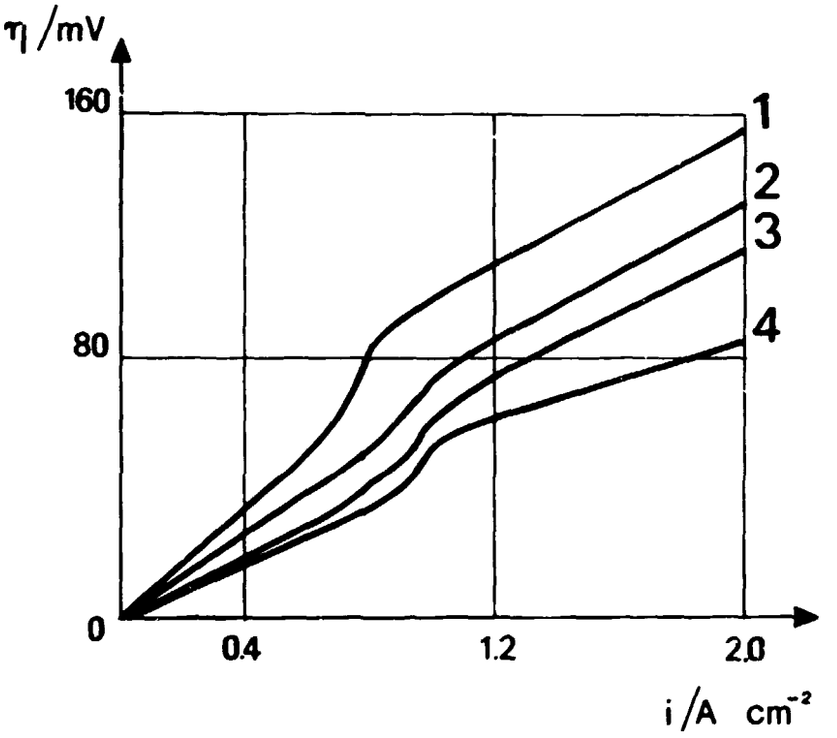

Fig.8.

1. 950 °C
2. 970 °C
3. 990 °C
4. 1010 °C

Aluminium deposition is interpreted as a limiting current phenominon. A plot of E versus log $\frac{i_d - i}{i_d}$ yielded a straight line with a slope $(\frac{RT}{nF})$ corresponding to n = 2.81-2.96

The sodium content of aluminium is found to increase drastically to 0.4 wt% Na independent of the cryolite ratio in the limiting current range. The cathodic overvoltage is not influenced by alumina content, in the melt, but it decrease strongly with increasing cryolite ratio.

The charge transfer overvoltage is found to be only a few mV. The change transfer resistance indicate 3 electron process.

It is established, chemical reaction preceeding or following electron transfer is not. The major part of the overvoltage is attributed to the accumulation of NaF in a diffusion layer, which causes a negativ shift in the potential of aluminium electrode.

The species undergoing mass transfer are aluminium complex species which diffuse toward the electrode and the fluoride ion move opposite direction as is shown in Fig.9. (See Ref.2)

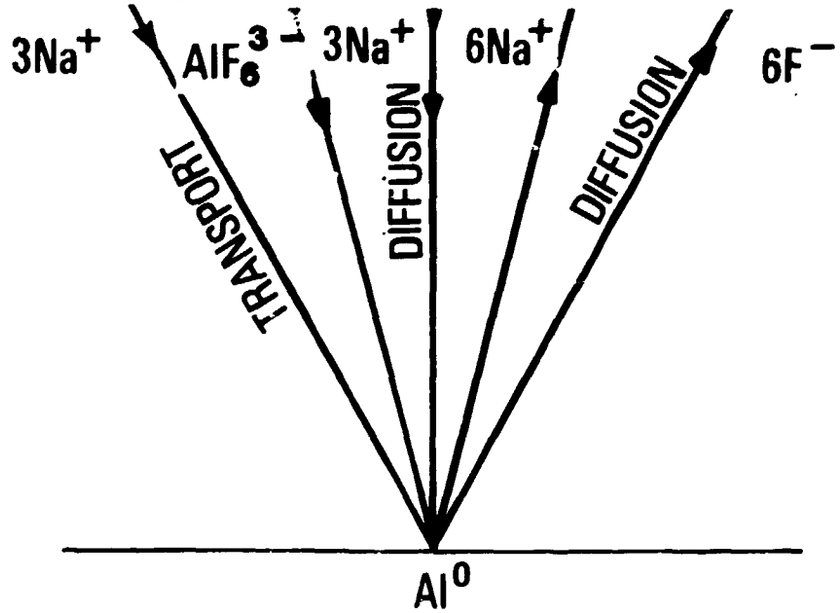

The overvoltage which is observed in the steady-state mesurements is attributed to the enrichment a NaF near the cathode, caused by the fact, that the sodium ion is the major carrier of charge. (19,20)

2.5. Anode consumption, aspects of anode performance

The overall reaction in the Hall-Heroult process with carbon dioxide as the primary product of the anode reaction gives a theoretical carbon consumption of 334 kg carbon per ton aluminium produced at 100 % CE. However, the actual consumption is subtantially higher and ranges from 420 to 550 kg.

The processes which contribute to this excess carbon consumption are:

- Electrochemical evolution of carbon monoxid.
  The exit gas contains CO, which form by a secondary reaction between CO_2 and aluminium dissolved in the electrolyte.
- Carboxyreaction.
  At temperatures from 950-970 ^{o}C carbon dioxid evolved $CO_2 + C = 2CO$ by the Boudouard reaction.
- Airburn.
  Excess carbon consumption is influenced by airburn, as following reactions $C + O_2 \longrightarrow CO_2$ at 400 ^{o}C and $2C + O_2 \longrightarrow 2CO$ at 550 ^{o}C.
- Dusting.
  The most important of the excess carbon consumed at the active anode surface is due to erosion of the material by selective oxidation of binder coke.

The main target of anode paste studies is to minimize excess consumption.

The anode excess consumption depend on

- the current density,
- anode paste composition, quality of raw material, coke and binder rate,
- additive and impurities in the anode paste.

It is established, that the anode consumption decreases as current density increases, because decreased the possibility of CO formation. The surface covered by anod intermediate product is activated and it sure more uniform consumption.

Anode consumption vs. current density is shown in Fig.10. (See Ref. 21, 22)

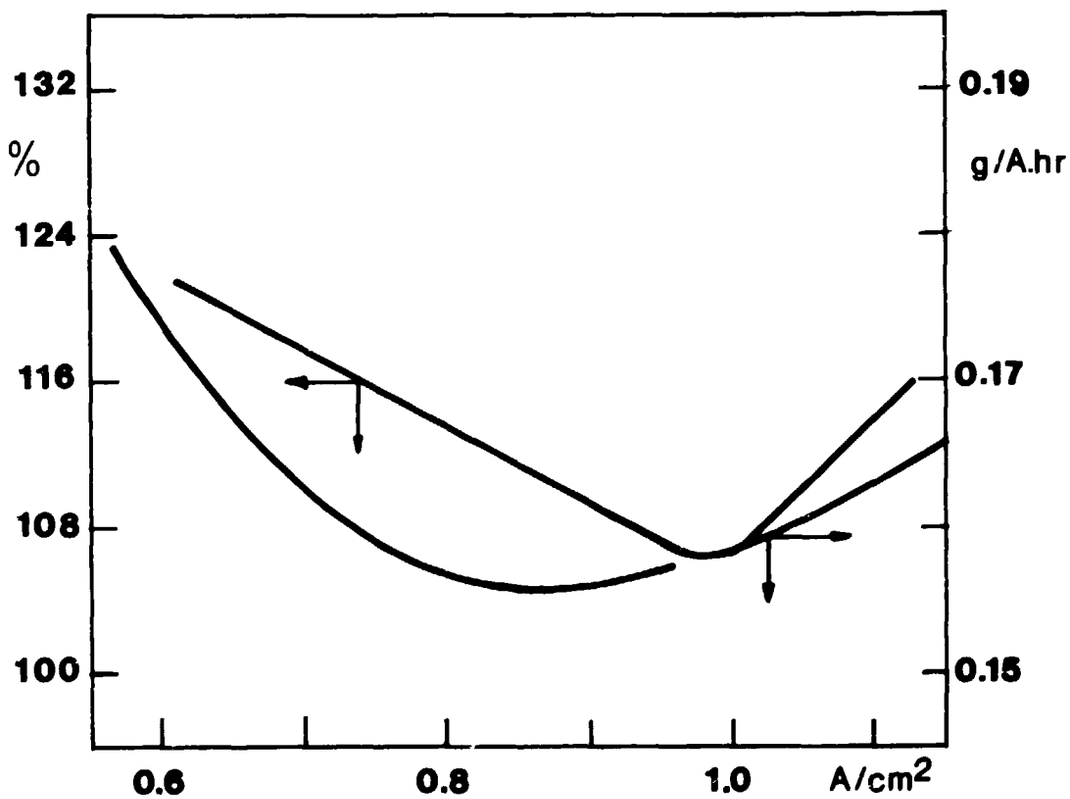

The laboratory tests have shown the anode consumption is difference at prebaked and Söderberg electrode.

Table 1.

			Prebaked	Söderberg
			g/cm^2h	
Airburn	at	500 °C	0.02	0.10
		700 °C	0.3	0.40
Carbooxy.	at	950 °C	0.012	0.02
		1000 °C	0.018	0.03

Significant effect of coke source, binder content, forming method and baking temperature is on the properties of prebaked anode.

For verifying of relationships, is interpreted, the anode consumption function v.s. raw material properties.

The anode consumption - calcination temperature relationship is shown in Fig.11. (See Ref.2.)

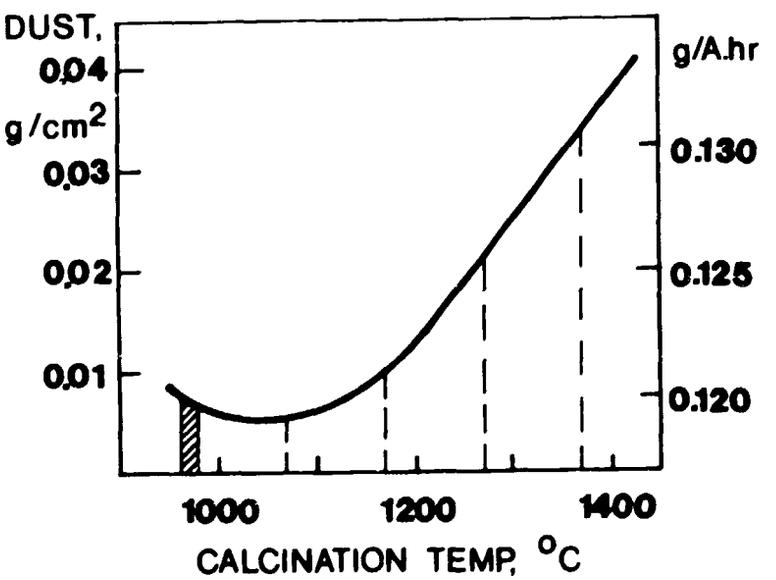

Coke properties is influenced primary by calcination temperature. Pitch content is a very important parameter is to adjustment the optimal anode paste composition.

The effect of pitch content on the different properties is shown in Fig.12. (See Ref.2.)

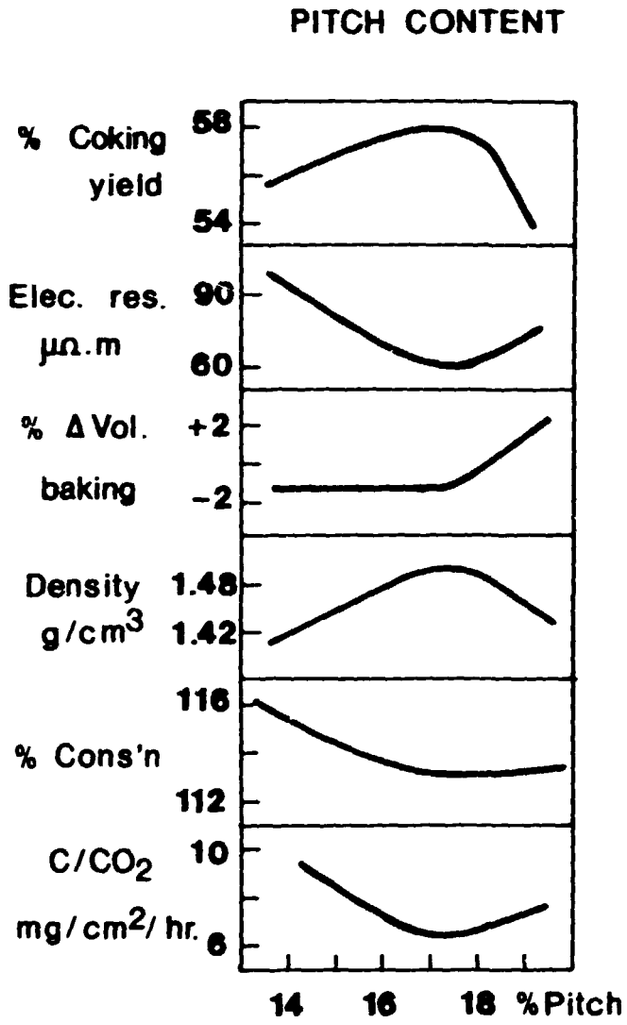

Fig.12.

Especially for Söderberg anode can be improve, so the anode consumption is decreased by additive in the anode paste.

The used inorganic additive change mainly the quality of the binding material.

It is found, that the addition of aluminium fluorid to Söderberg paste reduces anode consumption. (24, 25)

The reduction in anode consumption is attributed to the action of aluminium fluoride vapour with decreases the difference in reactivity between the binder coke and filler coke and resultant release of particles of filler coke.

3. CURRENT EFFICIENCY AND BACK REACTION

The rate of back reaction in aluminium electrolysis is important in current efficiency. The rate of dissolution of aluminium seems to be most important step is re-oxidation process. Several measurements of solubility of aluminium in cryolite have been made but the results are very dependent on the experimental method use.

3.1. Interraction between aluminium and the electrolyte

In the table is shown the free energy changing for the reaction between aluminium and electrolyte (26).

Table 2.

	Reaction	ΔG KJ/gekv at temperature 1227	1273	1323
1.	$Al+6NaF \longrightarrow Na_3AlF_6+3Na$	13.8	6.7	3.8
2.	$Al+\frac{1}{2}\ Al\frac{F}{3} \longrightarrow \frac{3}{2}\ AlF$	46.9	32.6	18.0
3.	$Al+Na_3AlF_6 \longrightarrow 2AlF_3+3Na$	134.0	131.0	73.0
4.	$Al+\frac{1}{4}\ Al_2O_3 \longrightarrow \frac{3}{4}Al_2O$	139.0	133.0	126.0
5.	$Al+5NaF \longrightarrow Na_3AlF_6+2Na$	-22.2	-17.1	-9.6

For these reactions a large number of investigations have been carried out.
The experimental methods employed are difference.

3.2. Test methods for the determination of aluminium solubility

The experimental methods employed include:

- visual observations
- chemical analysis in quenched melt samples
- weight-loss determinations
- vapour phase studies
- electrochemical measurements
- cryoscopy.

Color motion picture were used to confirm visual observations (27). When aluminium is added to the melt prior to electrolysis hydrogen bubbles arose profusely from the molten metal as it reacted with moisture dissolved in the metal. Identification of the bubbles as hydrogen is made by mass spectrografic analysis of the off gas.

Interraction between liquid aluminium and NaF is:

$$Al_{liq} + 3NaF_{(melt)} \longrightarrow 3Na_{(g)} + AlF_3 \qquad (3.1)$$

The relationship between ΔG and activity of AlF_3 and NaF is unknow. It is assume, that some reduced species are in dispersed form in the electrolyte.

The chemical method is based an the withdrawal of samples from the melt, which in contact with aluminium. During cooling the dissolved metal precipitates as a finely divided phase. The content of dissolved metal can be determined from the volume of gas evolved, when the crushed electrolyte sample is treated with hydrocloride.

In the weight-loss method is assessed the weight loss of a piece of aluminium added to the melt. In this case evaporation losses occur, the loss should be measure as a function of time. The extrapolated value to zero time gives the metal solubility. As crucible is opened, the metal losses due to oxidation by air and reaction with crucible material can be cause considerable error.

The weight-loss method indicate a higher value of solubility than those found by analysis of quenched samples.

It is known the vapour pressure above the cryolite melt is increased when aluminium is added. Some investigations have been carry out in order to determine the vapour pressures and the nature of the volatile species that contain the metal.

Several reaction shemes have been proposed

$$Al_{liq} + 3NaF_{liq} = AlF_{3liq} + 3Na_g \qquad (3.3)$$

$$Al_{liq} + 6NaF_{liq} = Alf_{3liq} + 3Na_2F_g \qquad (3.4)$$

$$2Al_{liq} + AlF_{3liq} = 3AlF_g \qquad (3.5)$$

It is assumed, the existence of the gaseous species Na_2F has not been interpret and aluminium monofluoride is known to be stable in gas phase.

The vapour pressure above $NaF-AlF_3-Al$ melt is shown in Fig.13. (See Ref. 28)

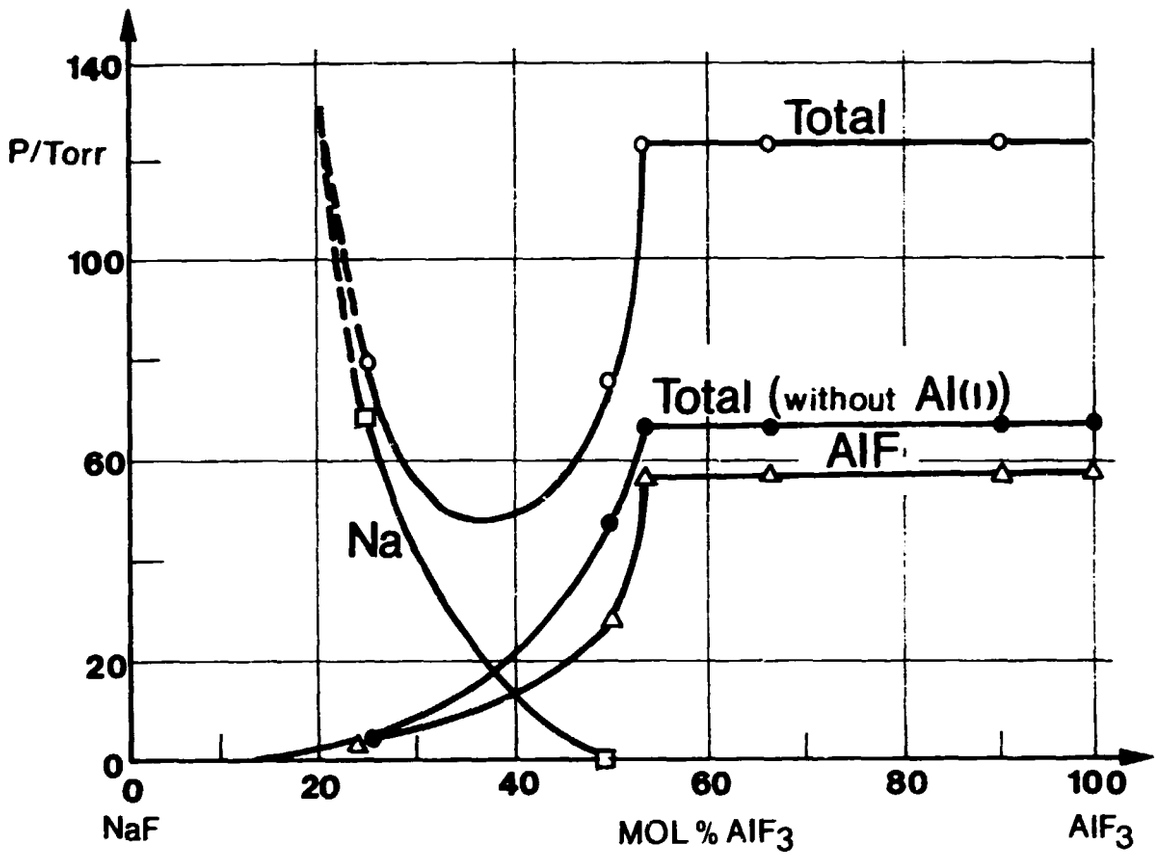

VAPOUR PRESSURES IN THE SYSTEM $NaF-AlF_3-Al$ at 1028°C

Open circles: Total vapour pressure with Al [1] present
Filled circles: Total vapour pressure without Al [1] present
Squares : Partial vapour pressure of Na [g]
Triangles : Partial vapour pressure of AlF [g]

Fig.13. (See Ref.28.)

Presently, on the base of vapour pressure it seems justified to assume that the metal-containing species are Na and AlF.

Metal dissolved in cryolite melts can be oxidized anodically on platinium electrodes. Well-known, that the electrolysis can be maintained at low current density between platinium anode and a aluminium cathode at potentials below the decomposition potential of alumina

The limiting current is observed which is a measuring of concentration of oxidizable species. On recorded polarization - curves by potential sweep may be observed limiting current density for anodic oxidation of dissolved aluminium.

The polarization curves recorded at 1000 ^{o}C in the cases of pure aluminium and aluminium+copper alloys on Pt electrode is shown in Fig.14. (See Ref. 29.)

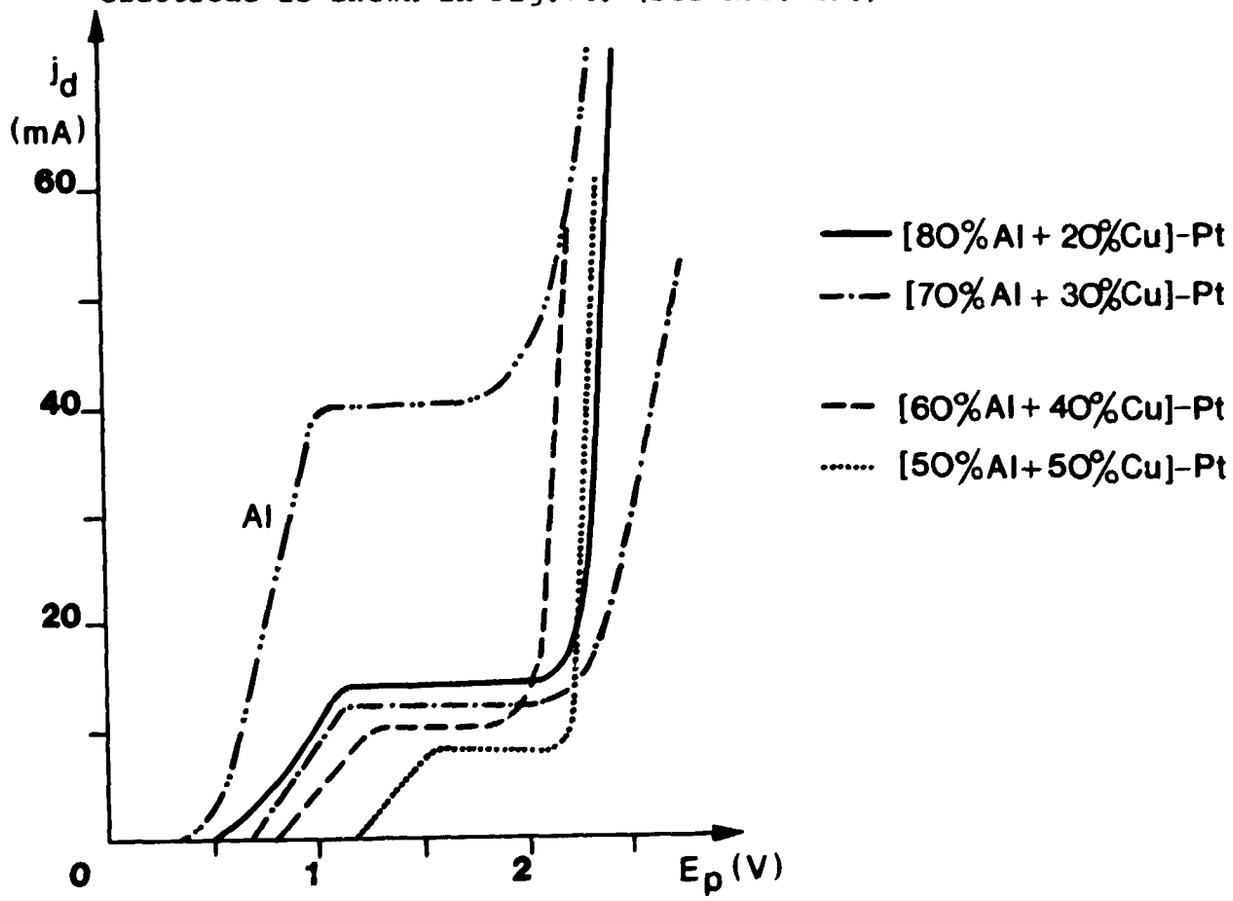

These polarization curves may be one explanation, that the dissolved metal formed at the cathode is being reoxidation on Pt electrode. The recorded current-voltage curves indicate limiting current for anodic oxidation of dissolved metal and its is influenced by aluminium activity. The activity of aluminium is varied by using Cu-Al-alloys.

Comparing the curves it can be seen, that the value of limiting current is the highest when applying the Al-cathode. At highest aluminium content in the cathode alloy, the value of limiting current also increase. This indicates, that the increase of copper content in the cathode alloy decreases the dissolving of aluminium as well as the reoxidation process following the former one.

The calculated value of change of charge number is equal ∿ 2. From this value it can be concluded, that the reoxidation of dissolved aluminium proceeds in some kind of electrochemical process with Z = 2. The $Al^{+} \longrightarrow Al^{3+}+2e$ reaction seems as the most probably one.

3.3. Reaction between CO_2-CO and dissolved metal

In principle different reactions can occur between gas and dissolved metal: (26)

Table 3.

Reaction	ΔG KJ/gekv 1223 °K
1. $Al+\frac{3}{2}CO_2 \longrightarrow \frac{1}{2}Al_2O_3+\frac{3}{2}CO$	125
2. $AlF+CO_2 \longrightarrow \frac{1}{3}Al_2O_3+CO+\frac{1}{3}AlF_3$	148
3. $Na+\frac{1}{2}CO_2 \longrightarrow \frac{1}{3}AlF_3 \text{ --- } NaF+\frac{1}{2}CO+\frac{1}{5}Al_2O_3$	175
4. $Na+\frac{1}{2}CO_2+\frac{1}{3}Na_3AlF_6 \longrightarrow 2NaF+\frac{1}{2}CO+\frac{1}{6}+Al_2O_3$	141

The mechanism of this reaction has been the subject of numerious investigations, but so far general agreement. Most of workers have assumed that reactions are metal dissolved in cryolite-alumina melts and gaseous or dissolved CO_2. There are several possible rate determining steps, but their indication demands very difficult experimental technique.

Among the several possible rate determing step the following three

- Slow dissolution of metal in the bath.
- Slow mass transfer of the dissolved metal through the bulk of the bath.
- Slow mass transfer at the interface metal/bath and bath-gas.

The rate of reaction can expressed as

- concentration of dissolved metal in quenching sample
- formation of CO (rfCo), determination of CO content in exhaust gases at given gas flowing
- determination of limiting current for anodic oxidation of dissolved metal.

In view of the complexity of process very helpful is to determinate CO, content in exhaust gases, the concentration of dissolved metal in the melt, limiting current for anodic oxidation of dissolved metal.

These laboratory scale-investigations were made, help for us knowledge of reoxidation reaction and give a good approximation to explaning of current efficiency.

Determination of rate reaction by quenching sample

The measurements were made without electrolysis and rate reaction was expressed as a rate of formation of reoxidation metal in melts, which can be found by quenching and determination of redissolved metal content by gas volumetric techniques.

Effect of variable NaF/AlF_3 an rate of reoxidation reaction.

Fig.15 shows the rate of reoxidation as function of CR. (See Ref. 30.)

The reason of uncertain relationships, is heating-up rate of furnace.

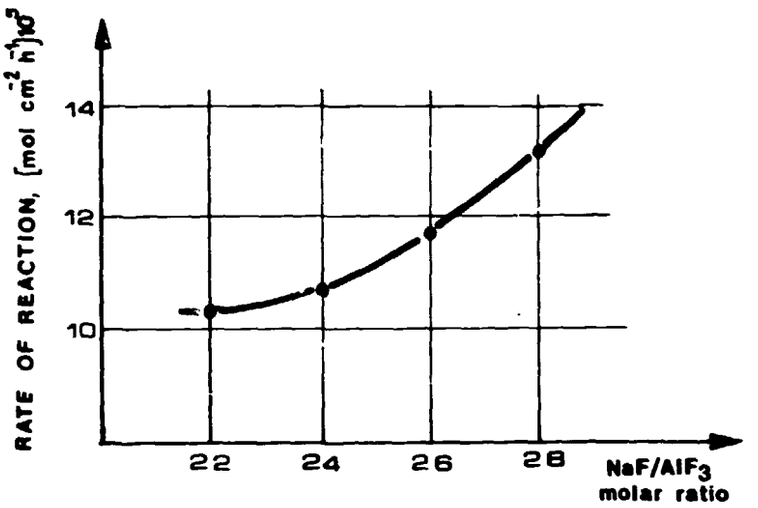

Rate of reoxidation reaction as a function of molar ratio at constant partial pressure CO_2

Fig.15.

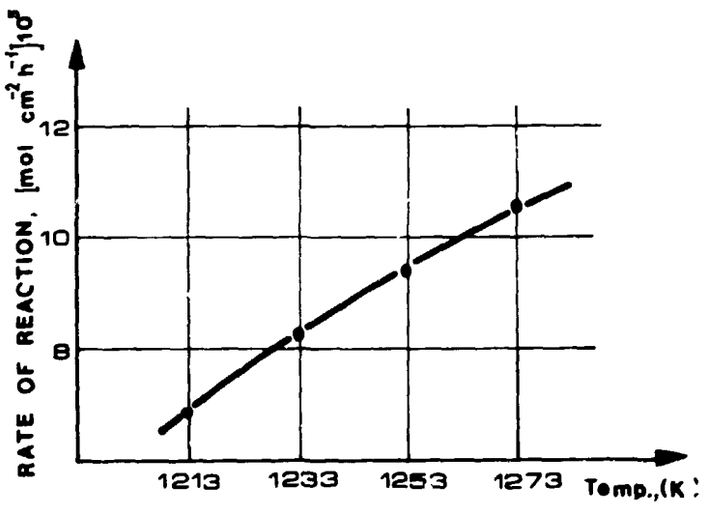

Rate of reoxidation reaction as a function of temperature in presence of CO_2

Fig.16.

At the effect of temperature Fig.16. results are shown on the base of magnitude of activation energy of reoxidation reaction, which is controlled by diffusion process.

The gas CO_2 bubbled the melt at different distance above metal interface when the depth of immersion of the tube (BN) was changed. Flow rate of gas was constant (3.6 l/h) corresponding the produced gas at 0.6 A/cm^2 anodic current density.

The results are shown Fig.17.

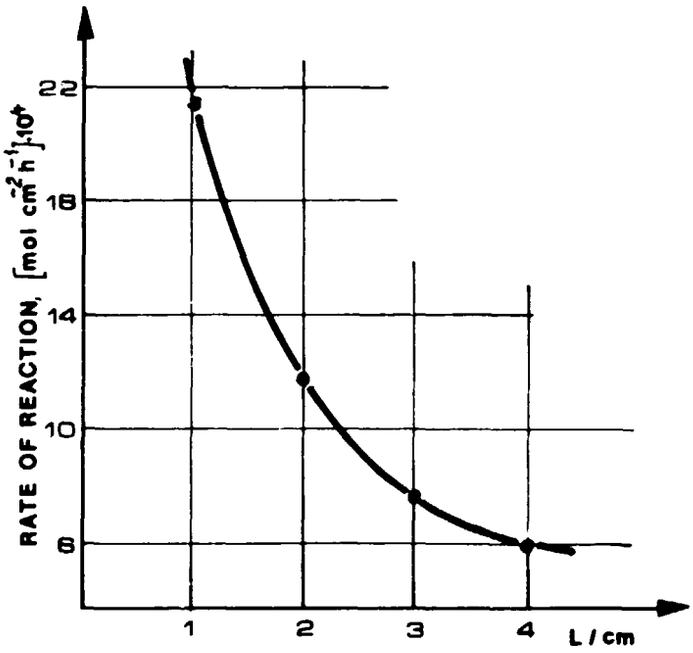

Effect of CO_2 gas induced stirring on the: rate of reoxidation process gas flow rate: 3.6 l/h.

Fig.17.

Rate of reoxidation reaction was increased by decreasing the distance to metal interface. Reproducible measurements is given when distance between depth of immersion of the tube and electrolyte level was always constant.

The strong effect of bubbling CO_2-gas on rate of reoxidation reaction certifies the existance of a mass transfer controlled process.

This indicates, that reoxidation processes are influenced by boundary layers.

Determination of reoxidation reaction rate by formation of CO.

- Experiments whithout stirring

Whithout external stirring the average value of rfCO is found to be $10.8\ 10^{-6}$ mol CO cm^{-2} min^{-1}. This average value is in fair agreement with data obtained by quenching method.

Rate of formation of CO (rf_{CO}) as a function of the temperature is shown Fig.18. (See Ref 31.)

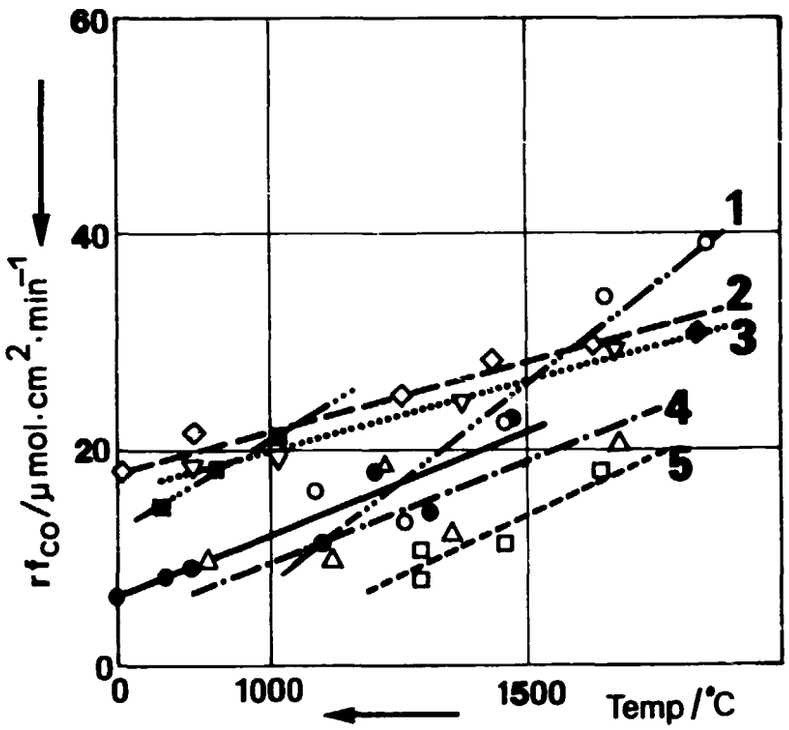

Fig.18. Rate of formation of CO(rf_{CO}) as a function of the temperature.

Open symbol: Ref.31.

- S. Gjerstad and B.J.Welch Ref.(32)
- Yu. I. Dvinin: Ref. (33)

The rfCO increase gradually with increasing temperature.

From Arrhenius plot (ln rf_{CO} versus $\frac{1}{T}$) can be estimated the activation energy which to be about 50 KJ/mol. Arrhenius plot of the rf_{CO} can be see Fig.19. at CR = 1($NaAF_4$).

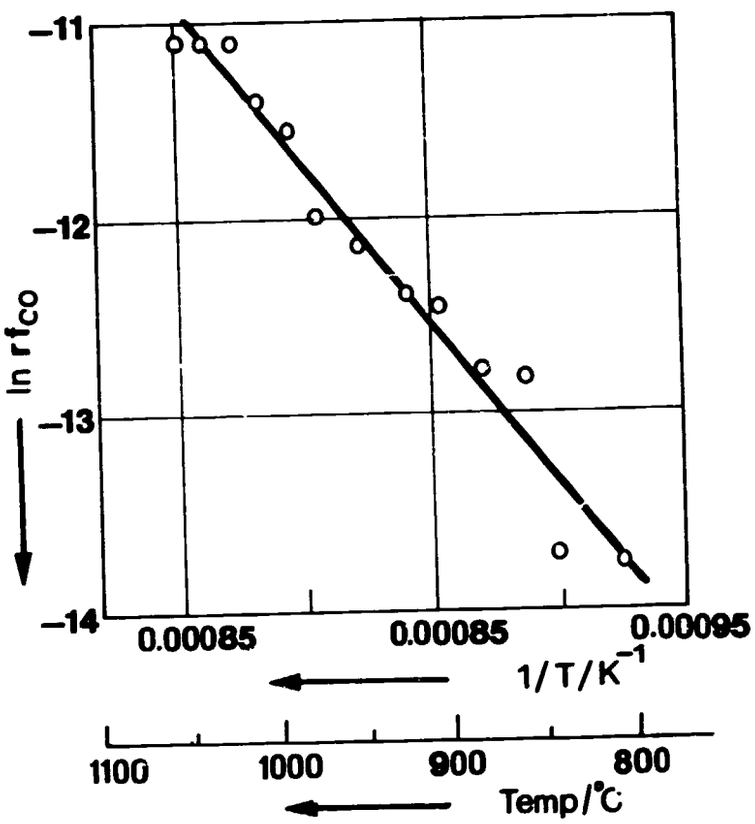

Fig.19. Arrhenius plot of rf_{CO} (See Ref.31)

Experiments with mechanical stirring

When the melts is srirred with boron nitride stirring rf_{CO} increased.

The rf_{CO} depend on position of stirrer in melt as shown in Fig.20.

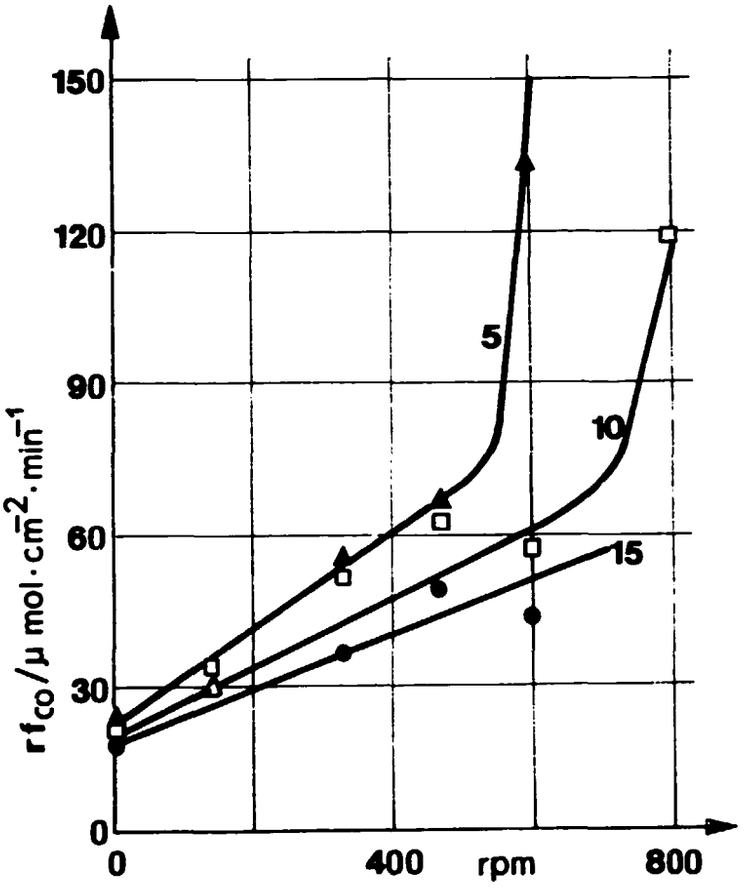

Fig.20. The effect of the speed of rotation of the mechanical stirrer on the rf_{CO}
Results obtained at 5. 10 and 15 mm above the metal surface (See Ref.31)

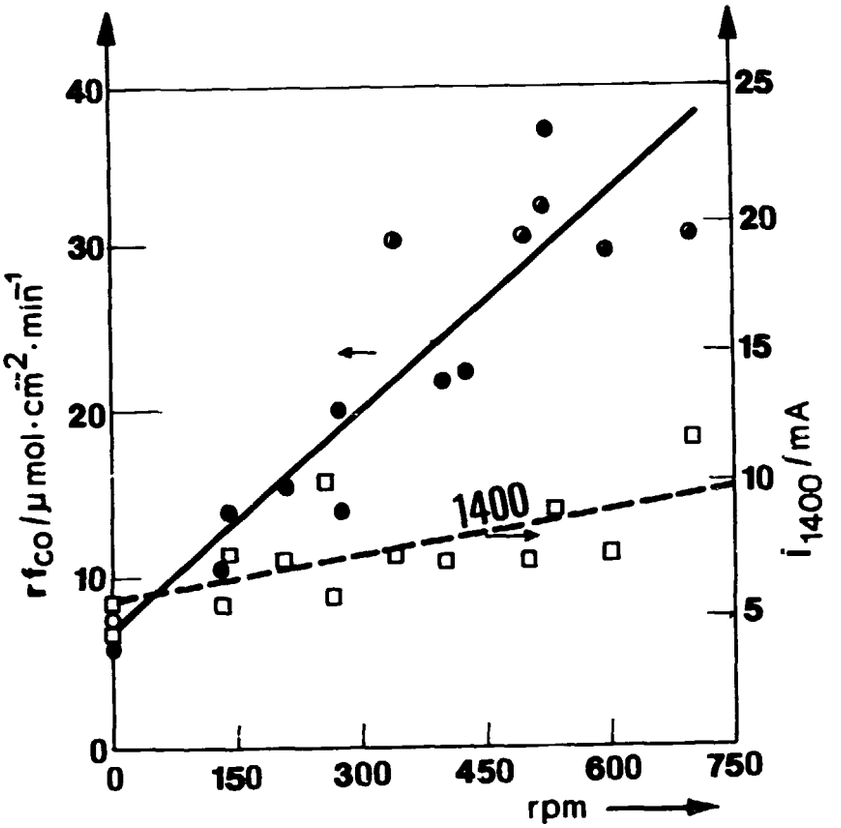

Fig.21. The rf_{CO} and i_{1400} as a function of the sped of rotation of the stirrer. The stirrer was 20 mm above metal surface.

Results given Figure 21. indicate that the concentration of dissolved increase with increasing rate of stirring, but no as markedly as for the rf_{CO}.

The effect of stirring increase when the stirrer is moved closer to the metal. The sharp increases observed at high rotational speeds are due to distortion of the metal surface.

Very interesting mention, when stirrer was immersed into the metal phase, the effect of stirring is less pronounced than with the stirrer locate in the melt close to the metal, as shown in Fig.22.

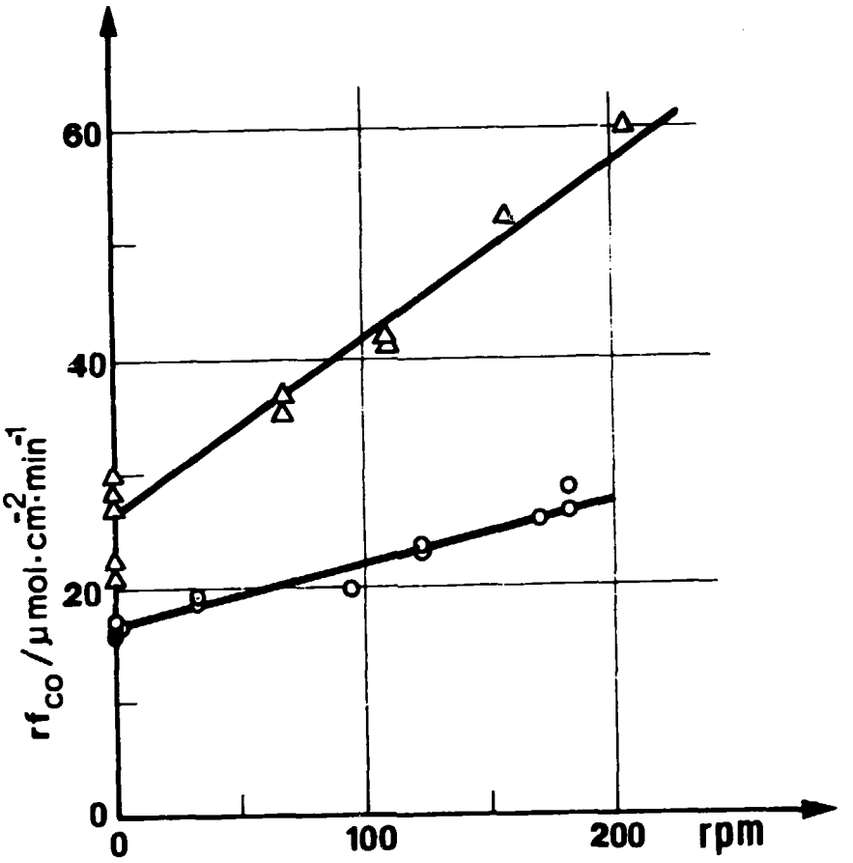

Fig.22. The rf_{CO} as function of speed of rotation of the stirrer.
Δ the stirrer located at 10 mm above the metal surface
O the stirrer located within the metal

Gas-Induced Stirring:

When the gas is bubbled through the melt rf_{CO} increase with increasing bubbling rate. In this case if the bubbling tube approche to metal surface in that case it is abroupt rise in rf_{CO}.

Determination of reoxidation rate by limiting current for anodic oxidation.

The limiting current for anodic oxidation give a good possibility, that for determination solubility of dissolved metal.

As indicated earlier the limiting current of anodic oxidation is proportional to aluminium activity in molten cryolite.

The limiting current i_e as function of depth immersion of Platinum electrode is shown Fig.23.

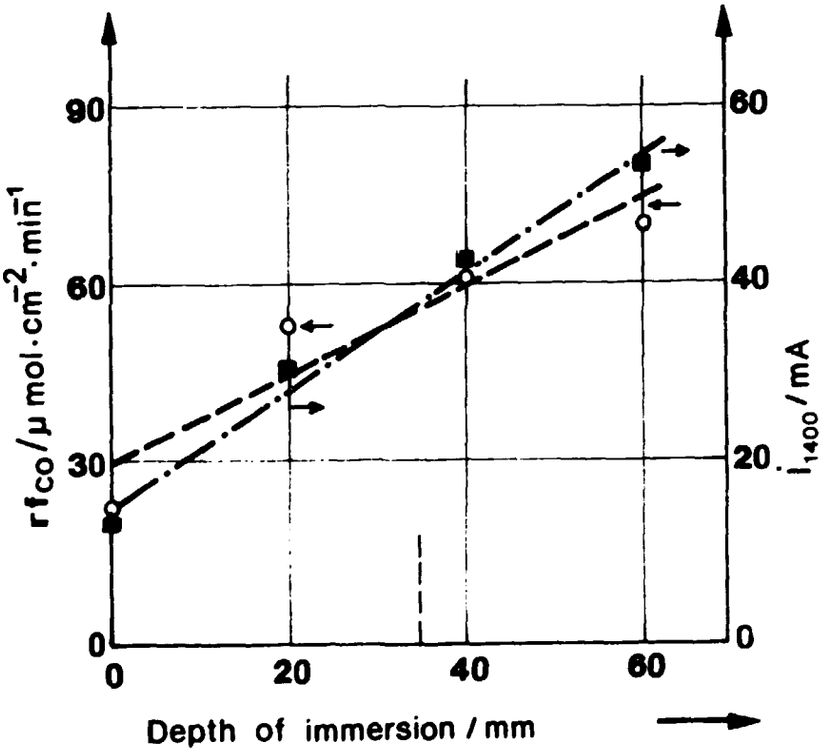

This indicates, that there exists no detectable concentration gradients with respect to dissolved metal within bulk of the melt.

Any gradients must be located in boundary layers at the interface.

rf_{CO} deincrease with increasing strirring rate, as shown Fig.24.

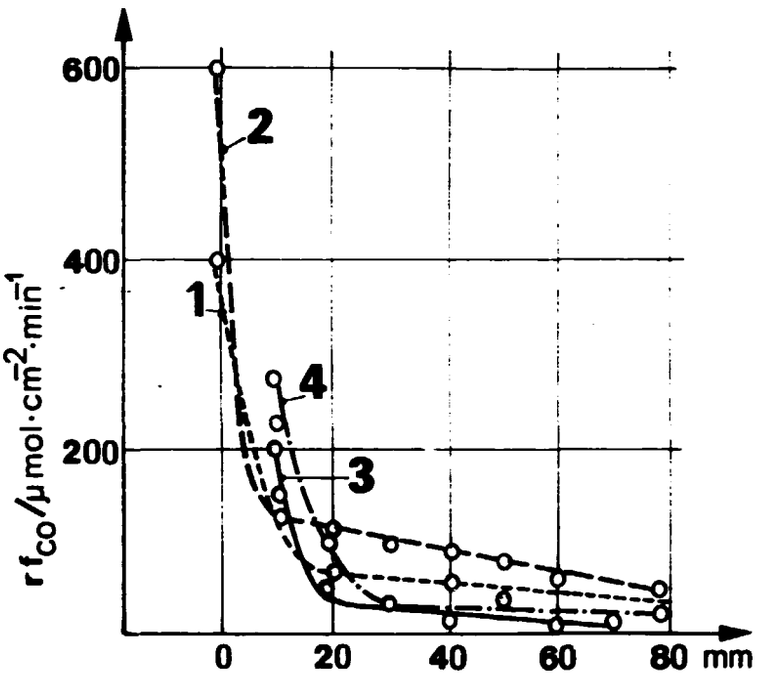

Fig.24.

The rf_{CO} as a function of the distance of the bubbling tube above the metal surface. Curve 1 - 65 ml CO_2/min.; Curve 2 - 55 ml Ar/min.; Curve 3 - 65 ml CO_2/min.; Curve 4 - 175 ml CO_2/min.

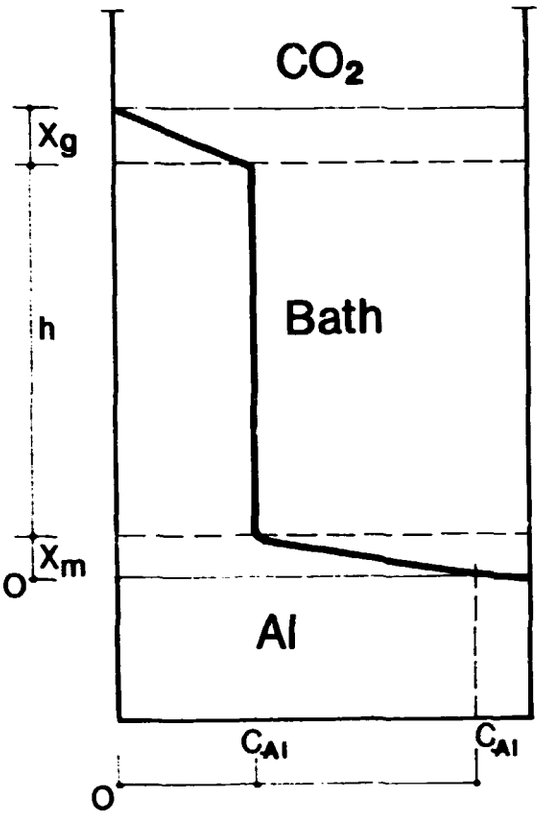

Fig.25. Proposed concentration profile of dissolved metal in the bath when CO_2 is present above the melt.
The thicknesses of the boundary layers X_g and X_M are greatly exaggerated

See Ref. 31,34. On the Mechanism of the Reoxidation Reaction in ALUMINIUM ELECTROLYSIS

For this reason the rate determining step in the process may very well change when degree of convection is change..

In industrial cell there is considerable convection caused by magnetic forces and by gas evolution.

3.4. Aluminium reduction cell variables and operations in relation to current efficiency

It is stated that the current efficiency (CE) is governed by reoxidation of dissolved metal by the anode gas. The laboratory studies of reoxidation reaction have thrown some light on the mechanism of reoxidation process, and the influence of some parameters have been studies. In any case some caution is needed when using these results to predict trends in CE.

The experimental conditions differ those proceeding in an electrolytic cell. The convection patterns and the relative surface areas will be different.

The conventional method for determining CE is based on the weighed amounts of metal tapped from the cell. Due to the large metal reservior in the cell, this method can only give the average CE for periods of several months. Metal pad height is not a good indicator because freezing and melting of the side ledge changes the cavity dimensions.

The most common method for invertorying the aluminium is to add a measured quantity of impurity such as, silver copper, nickel, or gold. Analysis of the aluminium give an aluminium inventory of the cell provided the impurity has been evenly distributed in the metal.

Radioizotopes addition have been used for determination of aluminium inventory. A gold isotope with a half life of 2.69 days was found to be the most suitable.

Determination of aluminium inventory in operating cell is shown Fig.26. (See Ref.32)

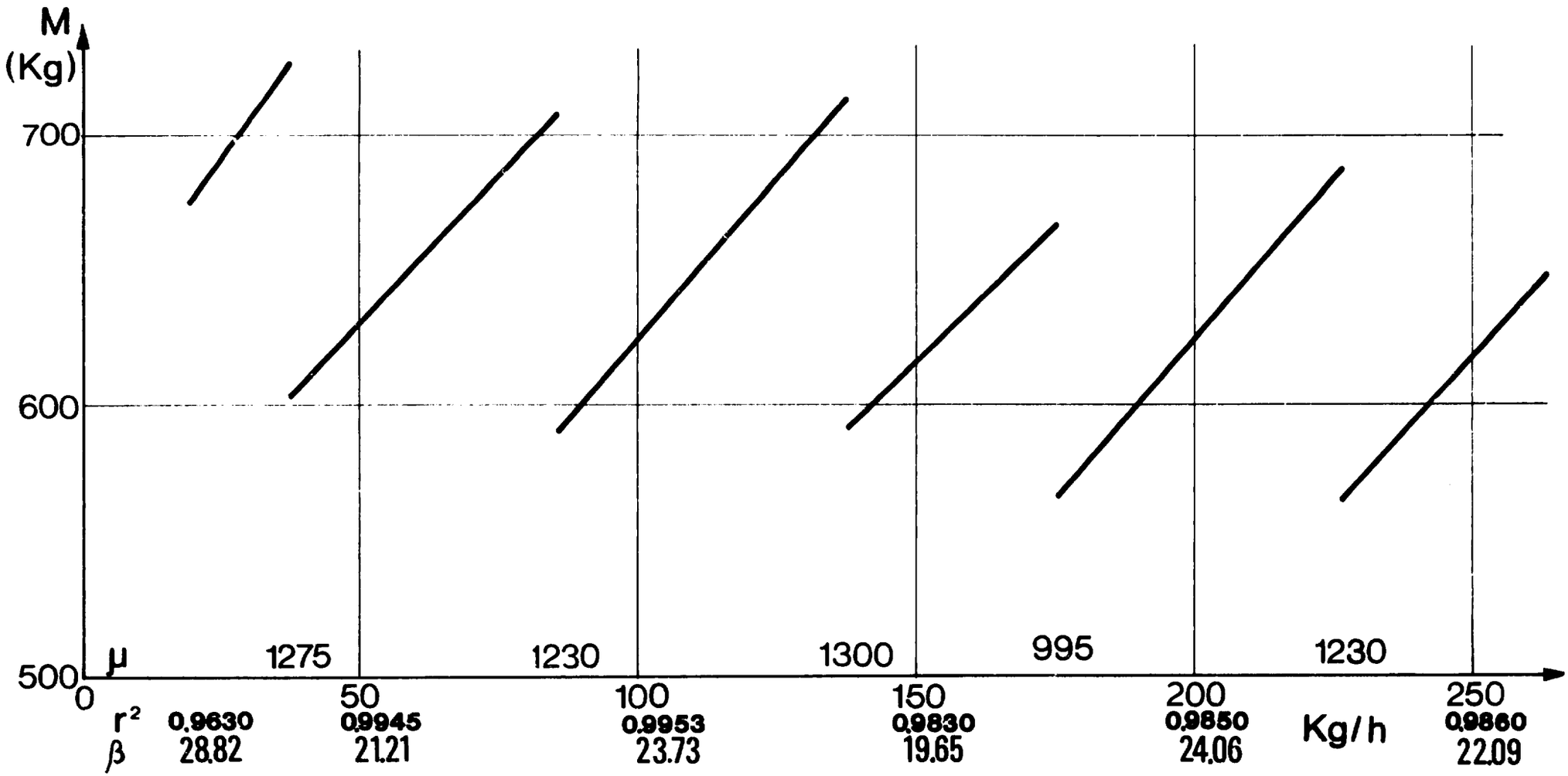

Fig.26. Aluminium inventory in operating cell

Gas analysis has been used shorter term or instantaneous current efficiency measurements. The common technique is to sample unburned, undiluted cell gas and calculate the current efficiency using the Pearson-Waddington relationship.

There are many possible errors in using the Pearson and Waddington equation. Aluminium can react with CO, forming alumina and carbon. CO_2 can react with carbon dust floating on the melt, forming CO. Air leaking into the hot gas sample not only dilutes the sample, but can oxidize some of the CO gas back to CO_2.

Hydrocarbons in the anode can produce hidrogen and methane in the off-gas. Hydrogen can react with CO_2, forming water and CO.

Beck modified equation of Person and Waddington to take into account some of additional reactions:

$$\%CE = g(50 + \frac{\%CO_2}{2}) - Z$$

Where g is the Boudouard reaction factor having a value of one for no reaction and two if the reaction goes to completion.

Other metal losses such as metal entering the lining or volatilizing from the electrolyte is reprezented by Z.

Hamlin's equation:

$$\%CE = |g(50 + \frac{\%CO_2}{2}) - z|\ |1 - z'|$$

Where Z' represents the fraction of aluminium loss by anodic oxidation of dissolved metal and electronic conduction. Beck found g to be a function of anode baking temperature varying between 1.07 at 960 ^{o}C to 1.02 at 1150 ^{o}C. Hamlin accounted for air burning of carbon and CO by the equation.

$$\%CE = \frac{100[\%CO_2+\frac{1}{2}CO-(0.268\%N_2-\%O_2)]\ (1-Z')}{\%CO_2+\%CO - \alpha C_A(0.268\%N_2-\%O_2-100(g-1)}$$

Where α is the fraction of the oxigen in the air that reacts with carbon and C_A the stoichometric factor for carbon in air burning.

$$(C_A)C + O_2 = (2-C_A)CO_2 + (2C_A-2)CO$$

Qui Zhuxian and Fong Naixiang analysed the above mentioned equations and their estimation for current efficiency; based on the unburned all gas composition

$$\%CE = 53.5 + \frac{\%CO_2}{2}$$

The influence of bath temperature is shown for laboratory (Fig. 27. and commercial cells (Fig.28). It is established, that the current efficiency decreases linearly with temperature.

Apperantly the slope is steeper in commercial cells than laboratory cell.

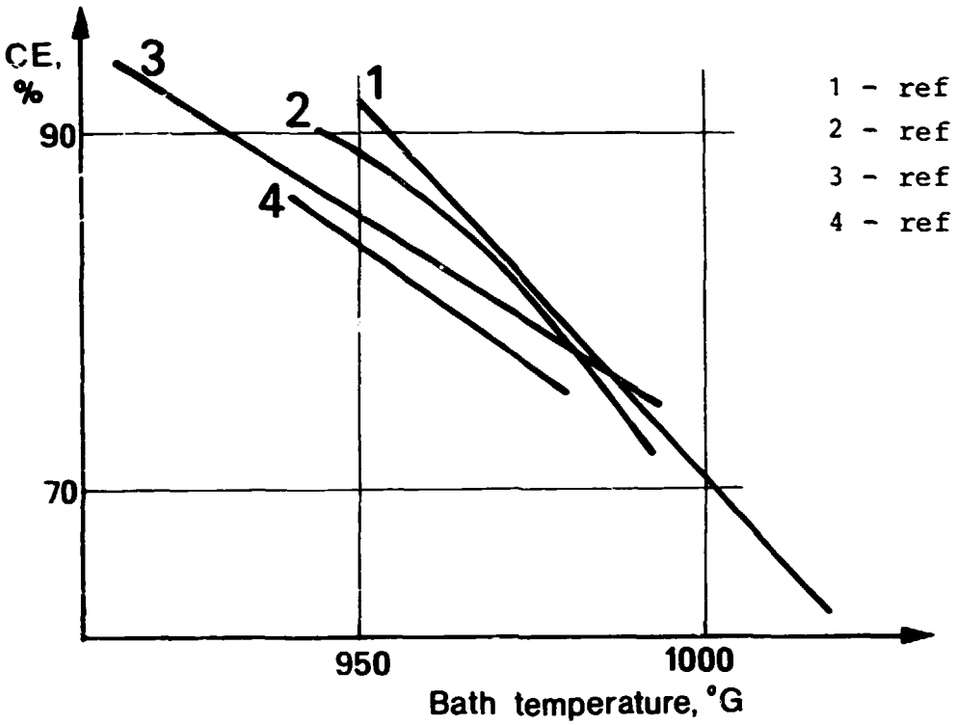

1 - ref.39.
2 - ref.40.
3 - ref.41.
4 - ref.42.

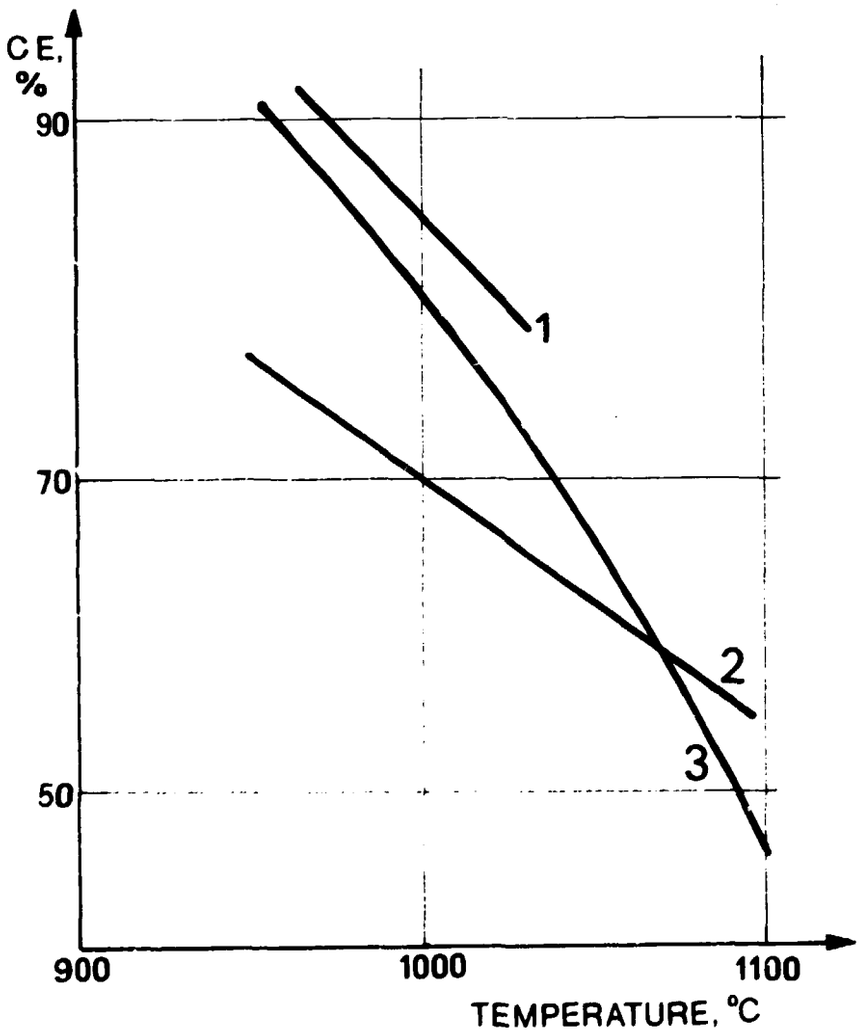

1 - ref.43.
2 - ref.40.
3 - ref.44.

The explanation is that a temperature increase in commercial cells will be followed by changes in other parameters, in contract the laboratory cells with external heating. A phenomenological explanation is that the rate at reoxidation process increases with temperature.

Bath composition

The influence of the cryolite ration is shown in Fig.29. for laboratory and in Fig.30. commercial cells respectively.

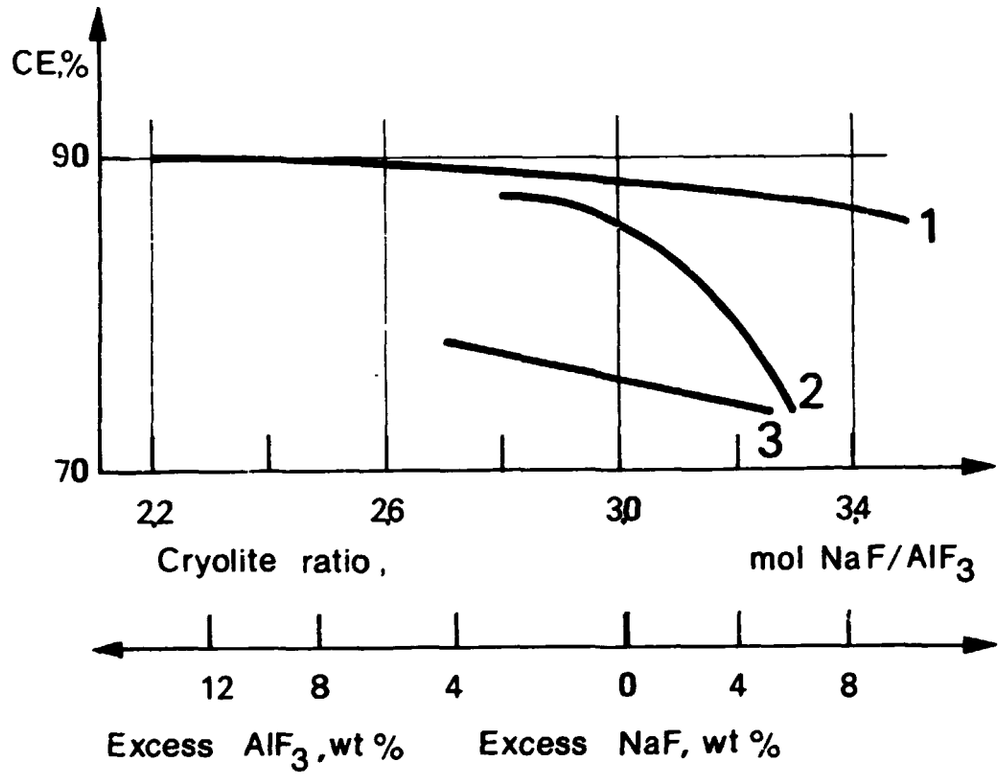

Fig.29.

1. Ref - 45
2. Ref - 46
3. Ref - 39

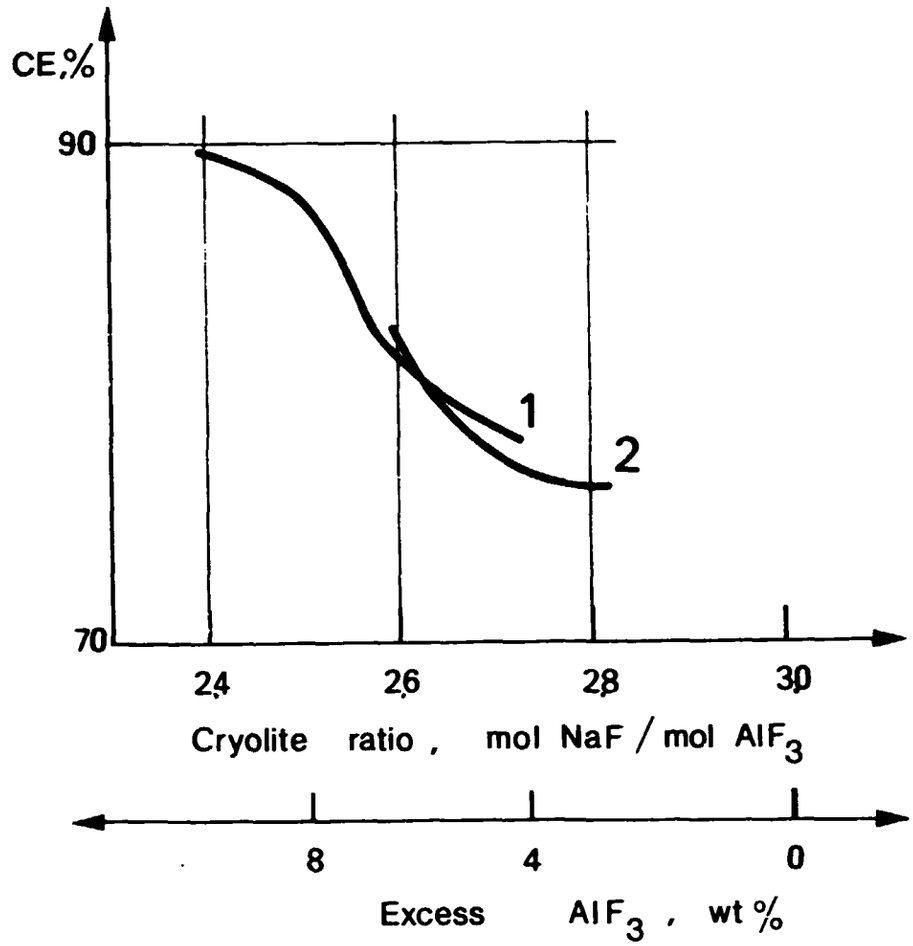

Fig.30.

1 - Ref 47
2 - Ref 48

Obtained results in laboratory and commercial cells indicate that the current efficiency increase with decreasing of molar ratio. This result is in a good agreement with relationship between rate of re-oxidation reaction and molar ratio.

Alumina content

The influence of alumina content is given in Fig. 31. for laboratory and in Fig. 32. for commercial cells, respectively. The slope of CE and the alumina content show a noulinear correlation.

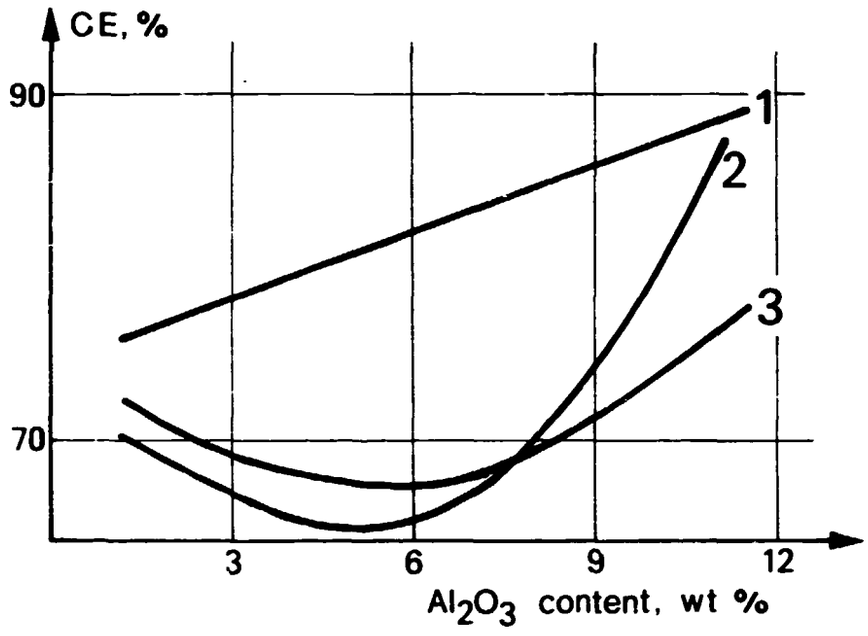

Fig.31. CE vs. alumina content in laboratory cells.

1 - Ref 41
2 - Ref 47
3 - Ref 49

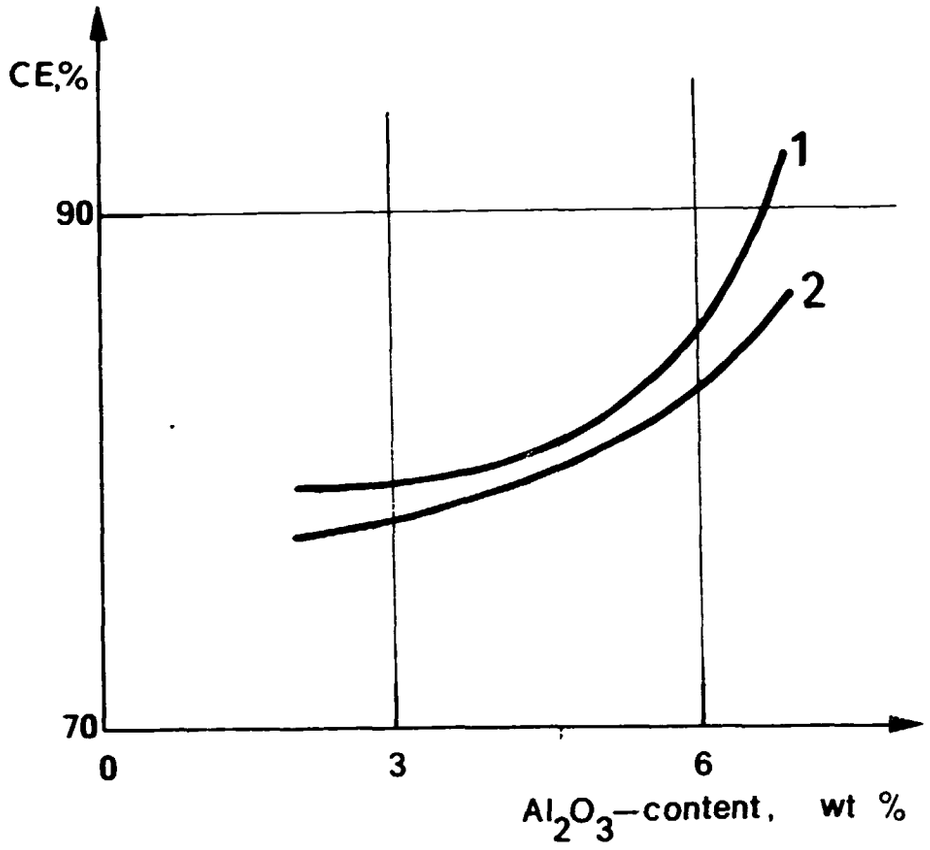

Fig.32. 1 - Ref 50
2 - Ref 48

The observed minimum in laboratory CE at about 5.0 s% will be moved towards higher alumina content when CaF_2 is added and towards lower alumina content when LiF is added. Analysing the dependance of reoxidation reaction on alumina content, it is established with the increasing of alumina content the reoxidation rate linearly decrease. The difference between the results obtained in laboratory and commercial cell is difficult to explain.

Interelectrode distance

The influence of interelectrode distance is given in Fig.33. for laboratory and in Fig.34. commercial cells, respecively. The results show, a decreasing effect on the CE when the interelectrode distance is decreased. The short electrode distance promote the recombination of the electrolysis products.

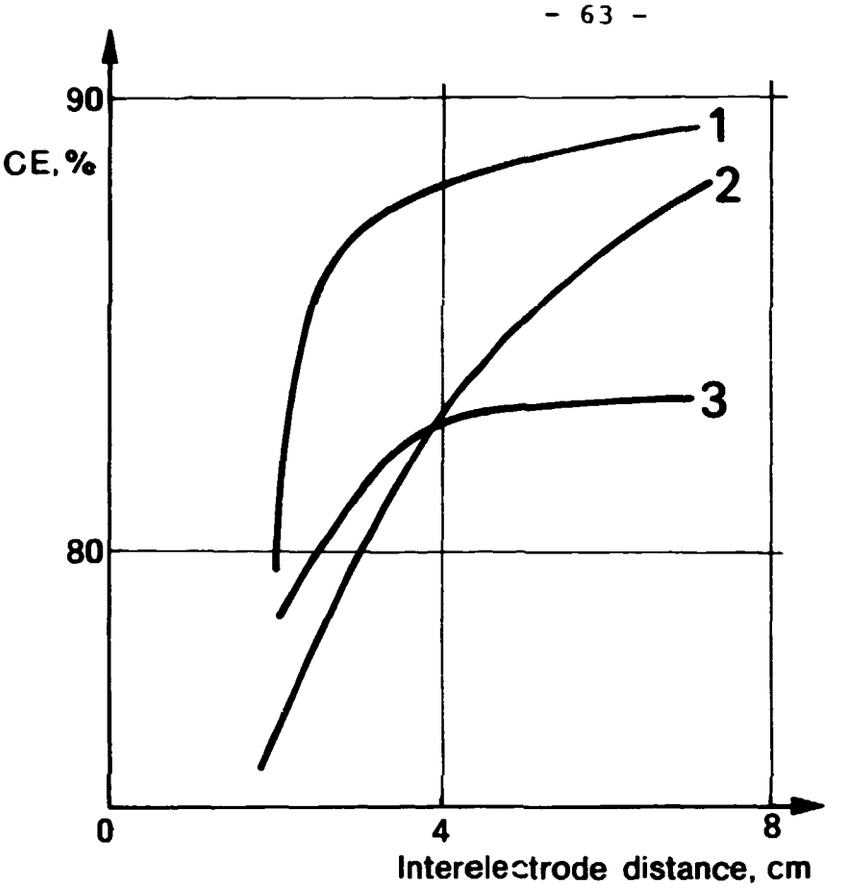

1 - Ref 51
2 - Ref 41
3 - Ref 52

Fig.33.

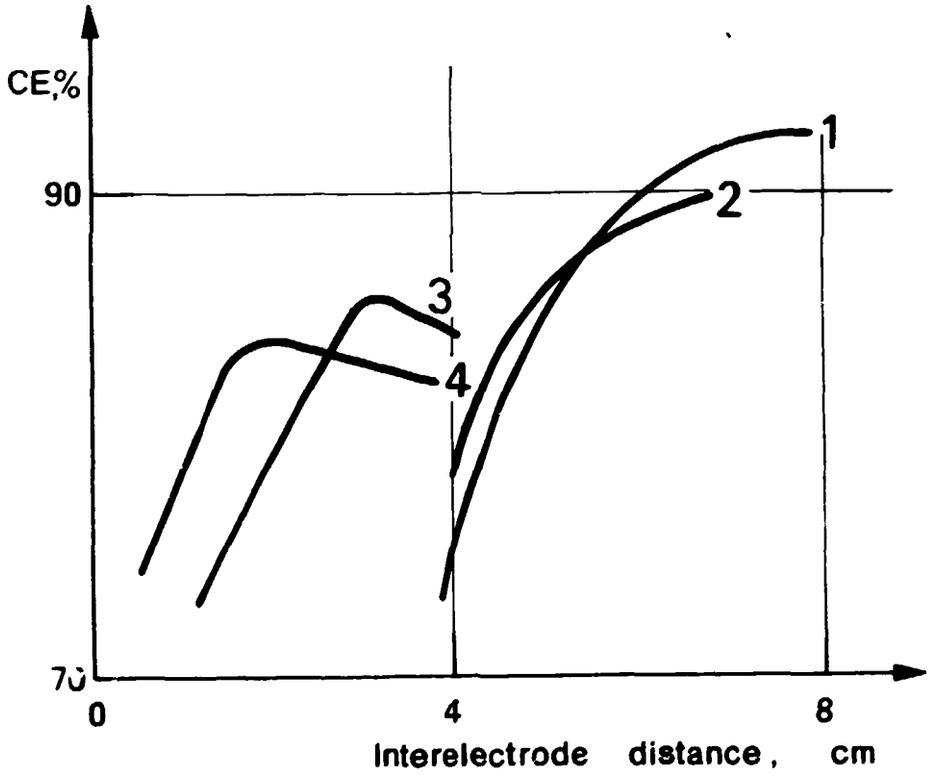

1 - Ref 53
2 - Ref 54
3 - Ref 55
4 - Ref 56

Fig.34.

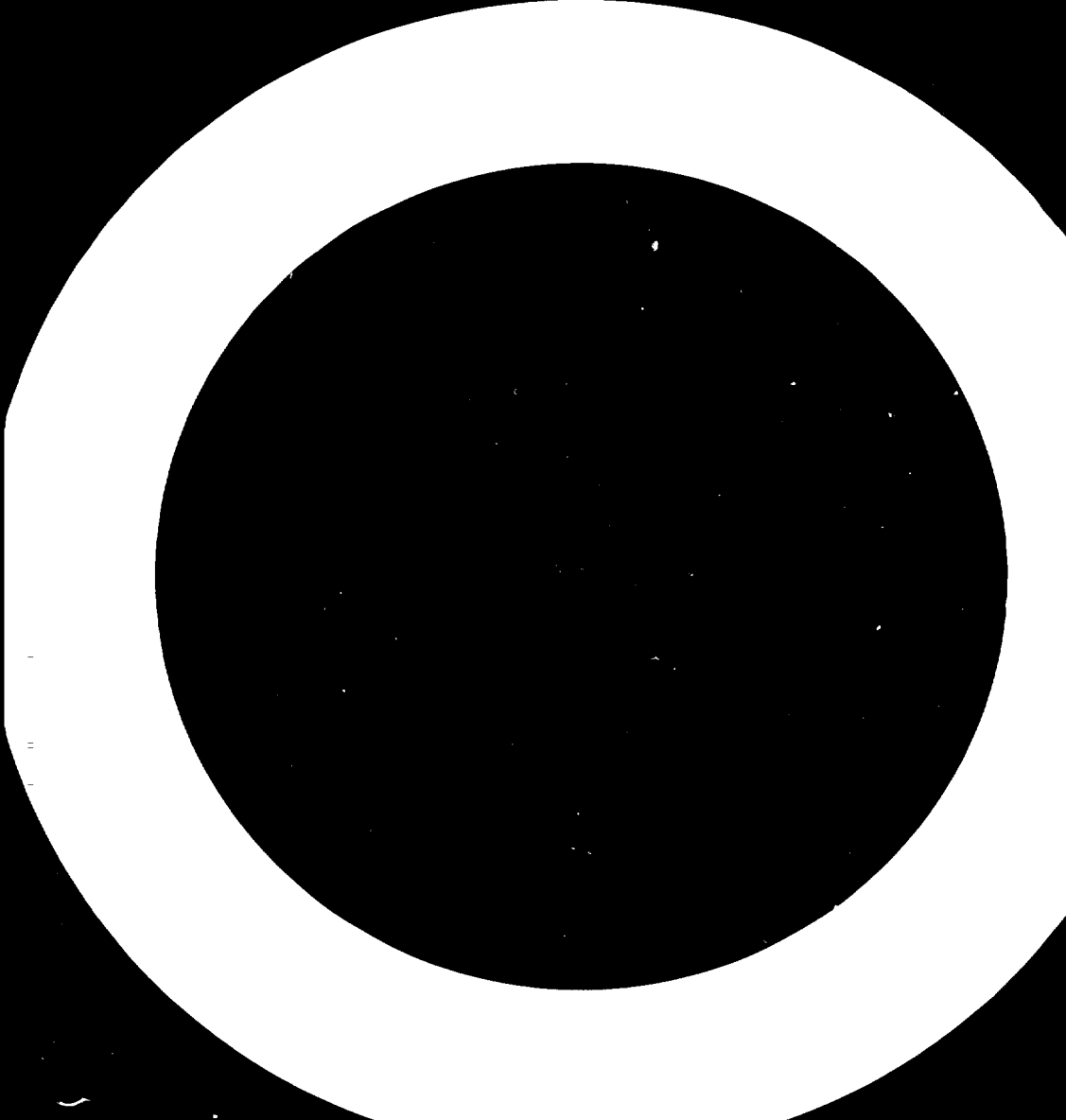

4. SOLUTION PROCESSES AND TRANSPORT PROPERTIES IN THE ELECTROLYTE

In order to minimize the sludge formation, the saturation solubility the rate of dissolution of alumina should be high. With the application of dry srcubbers, low temperature electrolytes, automation and energy conservation measures increase demands on metallurgical alumina. Even relatively small variations in the physical or chemical properties of alumina have been shown to cause major problems to the reduction operation.

4.1 There have been several studies relating to the kinetics of the dissolution of aluminas and each investigator has found the rate is dependent on range of variables.

Some workers have found a change in the dissolution rate when the alumina content increased above approximately 5 %. Kinetical measurements showed that below 5-6 wt% Al_2O_3 dissolution rate was independent of the amount of alumina already dissolved. These observations is explained by structural changes in the melt. When the percentage of oxide in the melt is low, additional oxide can be incorporated early. This incorporation becomes more and more difficult at higher alumina concentrations.

From the laboratory studies the general conclusion indicates a slow chemical reaction of the surface dissolution as a rate determining process when mass and heat transfer rates are speeded up by intensive stirring.

On the base of above mentioned the at simple chemical reaction, the reaction rate can be express.

$$r = K_o \exp\left[\frac{E}{RT_o}\left(1 - \frac{T_o}{T}\right)\right](C^* - C) \quad gcm^{-2}\ min^{-2}$$

This is an equilibrium reaction of the first order. At low concentration of oxide

$$r = K_o \exp\left[\frac{E}{RT_o}\left(1 - \frac{T_o}{T}\right)\right] gcm^{-2}\ min^{-2}$$

The kinetic parameters of alumina dissolution are shown

Table 4.

Author	k_o cm/min	T_o K	E kcal/mole	Range
Kachanovskaja	0.0747	1383	12.623	0.5 % Al_2O_3
			18.153	4.5 %
			25.932	9.0 % Al_2O_3
			37.602	12.0 % Al_2O_3
Gerlach	0.081	1383	16.055	α-Al_2O_3
	0.102	1383		γ-Al_2O_3
Thonstad	0.374	1383	19.706	T > 1342 K
			30.206	T < 1342 K

Laboratory studies established, that the total rate of dissolution is roughly proportional to the contact area. (57, 58)

In industrial practice is not possible to explain the alumina dissolution than, determining step rate by chemical reaction.

Only a part of alumina dissolves shortly after crustbreaking. One important restriction is set by the supply of heat. The alumina must be heated to the bath temperature, and what is more important, the solution process is strongly.

The remaining undissolved alumina can deposit at various locations in the pot:

1.) Become embedded in the top crust or rest on the top of crust.

2.) Settle along the side ledge above the metal level (on the side-breaking).

3.) Rest on the metal at the metal bath interface.

4.) Settle beneath the metal pad, forming a bottom sudge.

4.2 Measuring methods on alumina dissolution

To assess the rate of dissolution of alumina, the concentration of alumina should be determined as a function of time during the dissolution process. This procedure is difficult experimentally, and instead it is customary to determine the time of dissolution. The time needed to dissolve a sample of alumina powder in the melt.

The experimental methods used in laboratory investigations can be divided into following.

1.) Use of moderate stirring or no strirring:
With this method the driving force will be the concentration difference between the saturated layer and bulk.
This method is particulary suited for investigation of behaviour of alumina which has settled along the sides of peripherel channel in industrial cells.

2.) For study of the dissolution of alumina particles which are suspended in the melt, vigorous stirring can be applied.
The alumina particles become effectively dispersed in the melt and the dissolution of a small sample is completed in a few second. In this case the rate-controlling process is then different that suggested above. This method may be use to study the influence of various parameters on dissolution time.

3.) Reoxidation process, by addition of excess alumina to cryolite.

4.) In order to follow the dissolution process as a function of time, chronopotentometric analysis of the content of dissolved alumina is used.

4.1 Recently linear sweep voltametry is used to determine alumina concentration as a function of time the sludge dissolution. This is done at slow linear sweep rates (1.4 Vs^{-1}) and the slow dissolution enabled significant time intervals between consecutive measurements.

4.2 With application of fast seep rates (20 Vs^{-1}) alumina concentration is measured in range 1-5 sec intervals. For evaluating of alumina concentration is utilised both the change in the peak voltage and peak current by calculating the area under the curve from initiation of electrolysis to the onset of the anode effect.
Fig.35 indicates the calibration curve for determination of for alumina and sludge dissolution. (58)

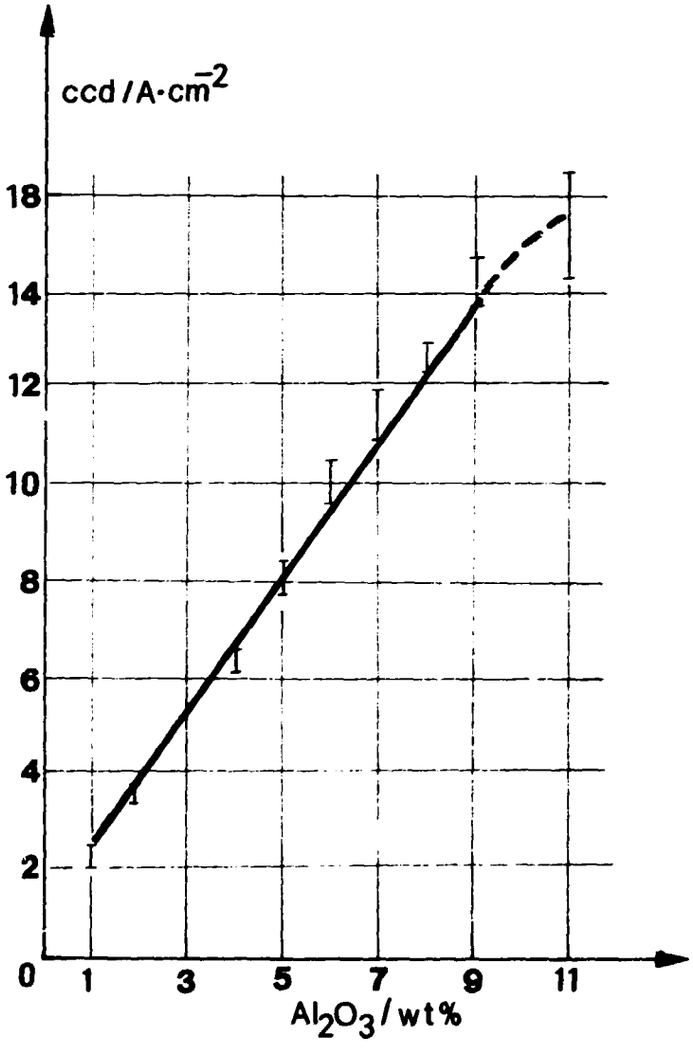

Fig.35.

4.3 Sludge formation:

As mentioned above alumina powder is dissolved in a stirred cryolite melt, the dissolution time is independent of the alumina content in the melt up to 5 to 8 % Al_2O_3, which is indicative of a zero order chemical reaction. The rate of dissolution of pressed tablets of alumina is found to be independent of the stirring rate over the entire concentration range, which also indicates reaction control. On the other hand, results of rotating disk experiment follow the laws of mass transfer control.

More difficult is determination of alumina solubility in presence of molten metal.

It is established, that the sludge formation accumulate on two part. One part of undissolved alumina accumulate at the interface between liquid aluminium and the cryolite-alumina melts, due to the high interfacial.

Settling of alumina at the bath/metal interface plays a important part in the mechanism of alumina dissolution in commercial aluminium cells. Accumulation of undissolved alumina at the metal/electrolyte interface is of interest not only with regard to current efficiency, but in connection with alumina feeding. Compared to alumina present in the bottom sludge, an alumina layer floating on the top of metal will be in a more favourable position for dissolution in the bath.

The rate of oxidation of dissolved metal when CO_2 is passed over the melt, decrease strongly when excess alumina is added. With measuring the CO-content in exhaust gas can be study the formation of alumina layer of the top of metal.

The metal reoxidation reaction with CO_2 is stopped when excess alumina is added, because this alumina layer inhibite the dissolution of metal into the melt.

As shown in Fig.36 the rf_{CO} decrease gradually by each addition, and a stacioner value is attained after 10-20 minutes.

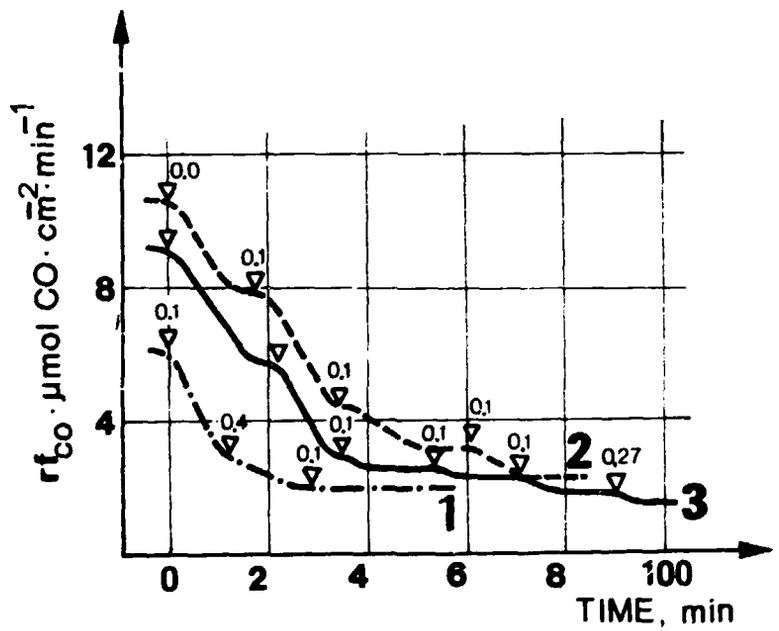

Fig.36. Changes in rf_{CO} by addition of excess alumina to cryolite-alumina(sat) melts in contact with aluminium. Amounts added per cm^2 cross sectional area indicated on curves for the three individual experiments shown, 1-1000 °C 2,3 -1020 °C (after Thonstad Light Metals 1980)

Studying the effect of mechanical strirring to be established, that when the stirrer was in the metal, the alumina additions on rf_{CO} is very slight.
As shown

Well known, the accumulation of large masses of sludge forming beneath the metal pad is harmful to pot operation.

Rate of sludge dissolution is in the bath phase measured base of the critical current density. The method was described erlier.

Dissolution of sludge in cryolite melts show in Fig. 37

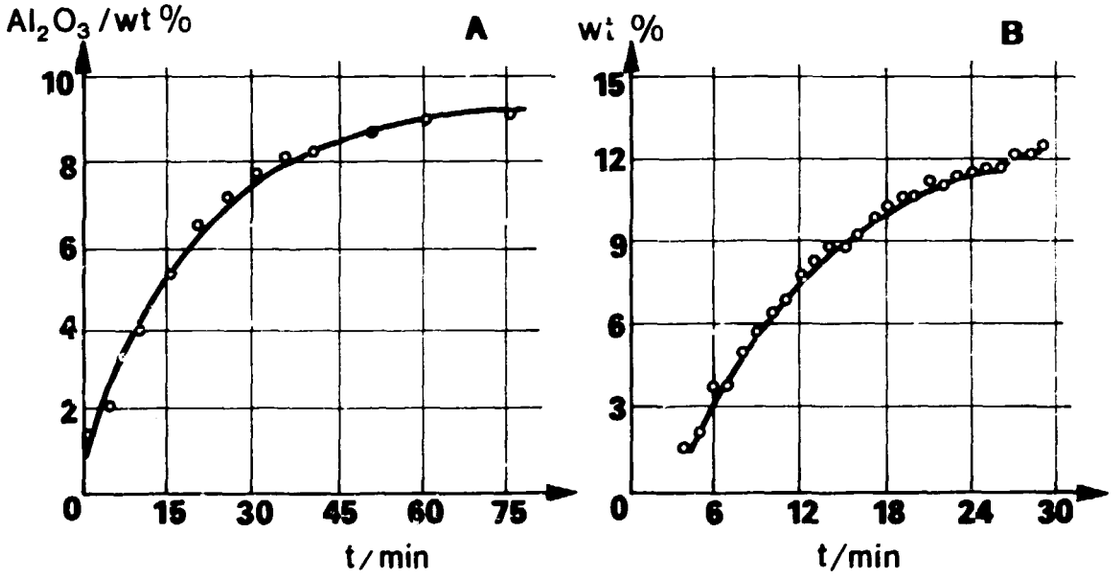

Increase in alumina content in cryolite melt exposed to settled alumina,
A – no stirring; B – stirring AT 40 RPM

Fig.37. Increase in alumina content in cryolite melt in contact with sludge.
(See Ref. J.Thonstad, W.Kristensen, Some properties of Alumina sludge Light Metals 1980) (59)

The rate constant is found to be K = 0.39 ±0.5 cm/min.

The dissolution process of sludge is changed in presence of aluminium layer.

Fig.38. gives typical curves obtained at mechanical stirring.

The laboratory studies shows that metal is surrounded by a film of bath along experimental crucible walls. The mass transfer of alumina takes place in this film.

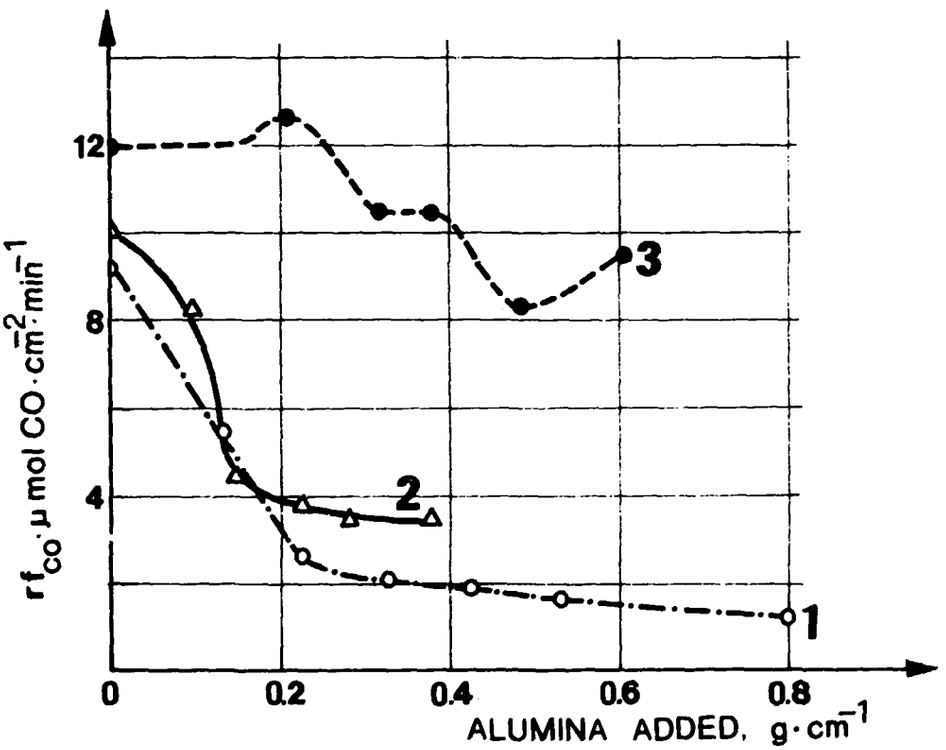

Fig.38. Effect of mechanical stirring on the rf_{CO} as a function of the amount of excess alumina added.

1 - no stirring
2 - stirring in the melt (125 rpm)
3. stirring in the metal (210 rpm)

(See Ref.31.)

4.4 Kinetical aspects of alumina dissolution and crust formation

Relatively small variations in the physical or chemical properties of alumina have been shown to cause major problems to the reduction operation. Studies for determinations of relationship is representeted between the physical properties of many Bayer aluminas and crust formation, dissolution.

Results is representated these different alumina. Two of which is sandy alumina was a extreme case of fluory alumina.

Physical properties of studied aluminas.

Table 5.

Alumina Description	Density kg/m^3 10^{-3}	BET surface area m^2g	α couter %	LOI 300 °C %	LOI 300-800 %
A. Fluid Bed calcined sandy	3.570	46.3	19	1.04	0.92
B. Rotary Kiln calcined sandy	3.547	77.4	23	1.84	1.00
C. Heavity calcined fluory	3.876	<1	80.9	<0.1	<0.1

Studies of the Alumina Dissolution at different physical-chemistry properties. (60)

Fig.39/1. presents the concentration versus time curve after addition of alumina. The curve typifies those obtained when the alumina disperses and does not term compacted aggregates. If the method of alumina addition or the process condition cause crustlike aggregation, then the dissolution curve exhibits two waves as illustrated Fig.39/2.

It should be noted, that all aluminas studied have exibited normal and two wawe dissolution.

Dissolution of alumina is influenced by-following parameters alumina type, bath super-heat temperature, amount of alumina added, α-content, alumina concentration electrolyte composition.

Most important fact of them are studied:

Bath Super-heat Temperature:

At given electrolyte composition for example, the super-heat temperature was lowered above just its liquidus temperature, in this case the dissolution time is found to be increased by approximately 50 %.

This is caused by insufficient super heat of the bath.

Freezing electrolyte generated around the alumina grains, which did not dissolve until sufficient had remelted.

Comparing the two sandy aluminas the major difference are in surface topografy and surface area.

Within the accuracy and repeatability of experiment it is difficult to indicate a major difference in dissolution rate between the two aluminas.

Contrasting with sandy aluminas, the dissolution time for fluory alumina under similar conditions is found to be about three times longer.

However with increasing the bath superheat (increasing of electrolyte temperature) dissolution time can be reduced to a value comparable with that observed for sandy alumina.

It can be seen in Fig. 40.

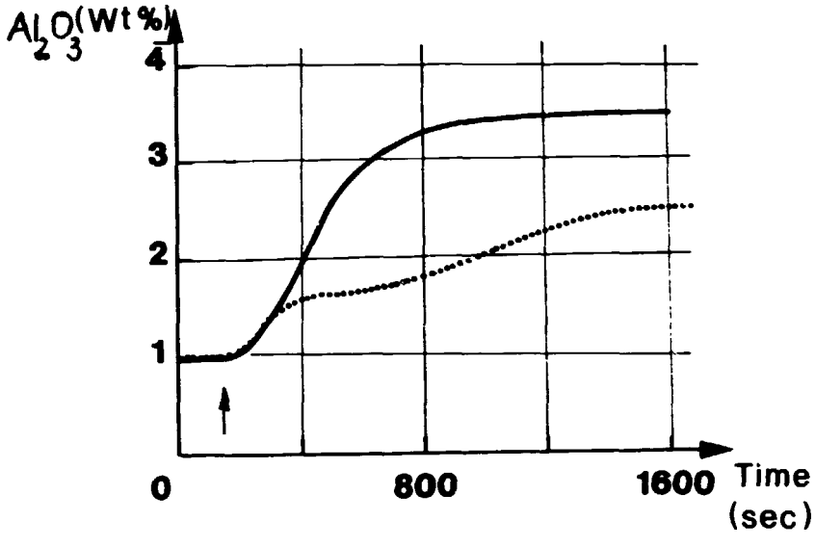

Fig.39. Dissolution curves showing normal (type A alumina) and crustlike aggregation (type B alumina) behaviour. CR = 1.35 CaF_2 = 5 wt% T = 988 °C

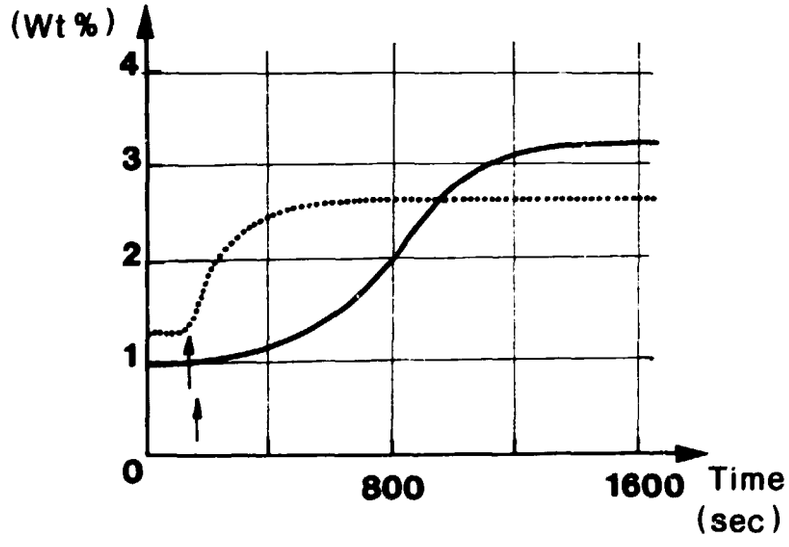

Fig.40. Dissolution curve (1) showing an extended dissolution time (type C alumina) at temperature T = 988 °C. Dissolution curve (2) showing a fast dissolution time (type C aluminium) at temperature T = 995 °C
(See Ref.60)

On the base of dissolution curves it is apparent, that provided the bath has sufficient superheat to prevent localized freezing, the alpha content is not important. However, the degree of superheat necessary to prevent the localized freezing is greater for the alpha form.

As seen the overall dissolution of low alpha aluminas requires about 20 % less heat than the crystallographically more ordered forms. Since the exothermic transformation can be mineralized by bath, the net heat absorbed by alumina during thermal equilibration will be less for sandy (low alpha types). Therefore they would not require as much superheat to ensure the absence of a frozen layer around the alumina particle.

About kinetic of alumina dissolution can be established:

The shortest dissolution time can be reach (the order 180s) for alumina which have been preheated to the least 800 ^{o}C and is well dispersed in the electrolyte.
The high surface area (low alpha content) aluminas tend to dissolve faster than the high alpha content alumina.

Heat plays an important role when the alumina added has not been preheated sufficiently or the bath has a low degree of super-heat. This is more evident for the dissolution of alpha alumina. Within a critical temperature region, the exothermic phase transitions to alpha alumina would be expected to favour the dissolution of sandy aluminas by lowering the heat required to thermally equilibrate.

This the particles are less likely to form a frozen electrolyte layer which passivates the dissolution. The thickness of any layer formed would be dependent on the alumina type, its temperature, and the degree of superheat of the bath. Particles thermally equilibrate rapidly as they fall through the electrolyte, but dissolution is dependent on presence of an alumina-liquid bath interface.

Comparison of the slow dissolution of sludges with the situation when crusting occurs supports the concept that some of the alumina undergoes a phase transformation to the alpha type. This could be through a mineralizing action of the bath within the sludge that is formed. It would result in reduction in surface area and less favourable heat transfer conditions for dissolution.

The nature of crust in the electrolyte is a very important form point of view of alumina supplying. The rate of dissolution of alumina from the sintered and densitied part of a crust is considerably than for loose powder.

A factor contributing to the slower rate for crusts is that there must be the delays for thermal equilibration of the interface and diffusion (mass transfer) while alumina is being released.

4.5 Formation of aluminium carbide

The formation of Al_4C_3 is highly unwanted in the Hall-Heroult process. The Al_4C_3 inclusions in liquid aluminium, causes loss in current efficiency and may possibly be an important factor in shortening the life time of pot by chemical attack on carbon lining.

Thermodynamicaly aluminium should react readily with carbon to form aluminium carbide.

$$4Al(l) + 3C(s) = Al_4C_3(s)$$

The Gibbs free energy for reaction at 1000 ^{o}C is -170 KJ.

Aluminium and carbon can be kept in permanent contact for a long time without a detectable reaction. This have been atributed to oxide formation on the aluminium surface.

In the presence of liquid cryolite, however, the rate of reaction increases.

Most of the Al_4C_3 formed is found at the carbon/ cryolite interface and less at the carbon/aluminium interface. This increase may be atributed mainly to the ability of molten cryolite to dissolve aluminium and further to a decrease of the interfacial tension at the aluminium/carbon boundary.

Aluminium carbide formation vs. the reaction time present Fig. 41 a pure cryolite melt and cryolite melt with addition 6.0 wt% alumina. (61)

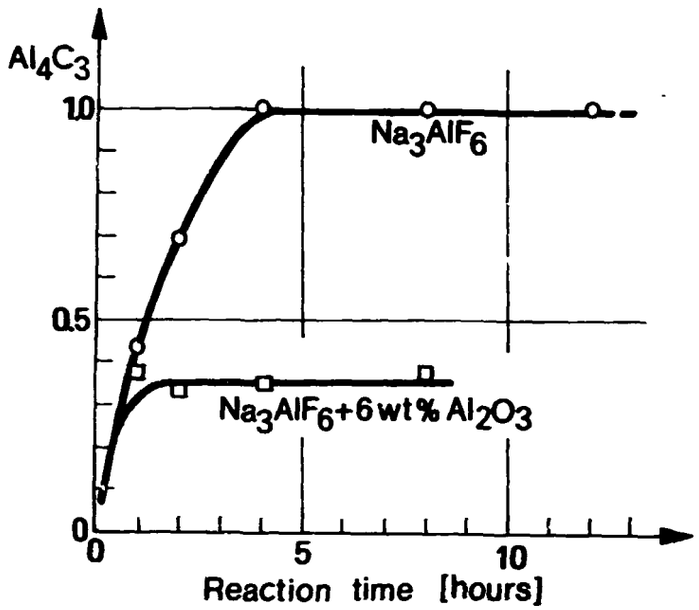

Fig.41. ALUMINIUM CARBIDE FORMATION v.s. reaction time for pure cryolite and cryolite-alumina melt at 6.0 wt alumina.

The curve for pure cryolite reach a constant level after 4 h reaction time, while the results with addition of 6 wt% Al_2O_3 shows that the maximum amount of Al_4C_3 is reached already after 1 h.

The kinetics for the formation of Al_4C_3 in pure cryolite suggests a boundary phase reaction, where a layer of Al_4C_3 is built up at the exposed carbon areas. Most of the Al_4C_3 produced is found at the interfaces between aluminium and carbon or aluminium and cryolite.

The carbide formation vs. the alumina content of the cryolite melt shows Fig. 42. (62)

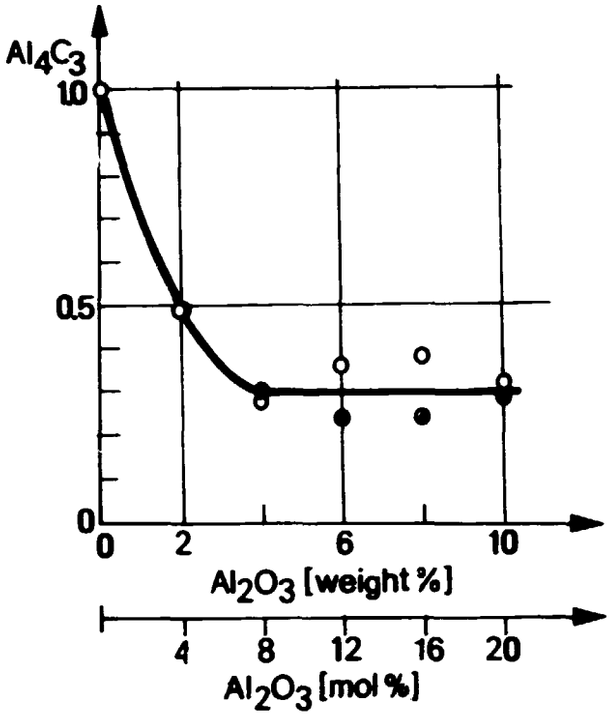

The important feature of this figure is the demonstration that the amount of Al_4C_3 does not change with the content of alumina above 4 wt%, but sharp increase in carbide formation is seen when the alumina content is decreased from 4 to 0 wt%.

During the electrolysis sodium and electrolyte are continuously being absorbed by carbon lining, creating problems of swelling of cathode. The chemical dissolution of carbon may be considerable, especially in those areas where, electrolyte, aluminium metal and carbon are in close contact and aluminium harvide is formed. The following

chemical reactives may be take place in the carbon lining:

$4Al(l) + 3C(s) = Al_4C_3(s)$

$4Na_3AlF_6(L) + 12Na(\text{in C}) + 3C(s) = Al_4C_3(s) + 24NaF(L)$

$4Na_3AlF_6(L) + 12Na(\text{in C}) + 3O_2(g) = 2Al_2O_3(\text{s.diss.}) + 24NaF(L)$

$4Na(\text{in C}) + 3O_2(g) + 2C(s) = 2Na_2CO_3(s)$

$Na_3AlF_6(\text{L, excess NaF}) + Al_2O_3(\text{diss.})$

$\longrightarrow Na_2O.11Al_2O_3(s) + Na_3AlF_6(L)$

$2Na(\text{in C}) + 2C(s) + N_2(g) = 2NaCN(L)$

As seen the sodium and carbon interraction is the most important factor influencing the cathode life. The sodium is not only electrochemically but it is entering into the cathode lining forming compounds. (63)

This probably continuous throughout the lifetime of the lining. The possibility of sodium formation according to eqution.

$Al(l) + 3NaF_{\text{in electrolyte}} = 3Na_{(\text{dissolved})} + AlF_{3\,(\text{in electrolyte})}$

The two theories exhibit for transport process of sodium through the cathode lining

- the vapour transport mechanism
- diffusion mechanism.

More credibility is the diffusion mechanism. Sodium reacts with grafite to form lamellar NaC compounds (C_8Na, $C_{64}Na$). The diffusion of sodium into cathode carbon material is very rapid in the initial stage of electrolysis. The diffusion constant for sodium is in the range $21\text{-}5\ 10^{-5}\ s^{-L}$.

It is established experimentally that during the operation of an aluminium cell, a progressive graphitization occurs in the carbon lining.

The recrystallization of carbon is usually extremely slow at temperatures below 2000 ^{o}C, it is believed that the graphitization is catalysed in the pressure of metallic sodium. The progressing graphitization reduces the rate of sodium absorption. The carbon material in aluminium cells consists mostly of amorphous or low graphiticied antracite in the start-up period of a new cell when most of the sodium absorpiton takes place.

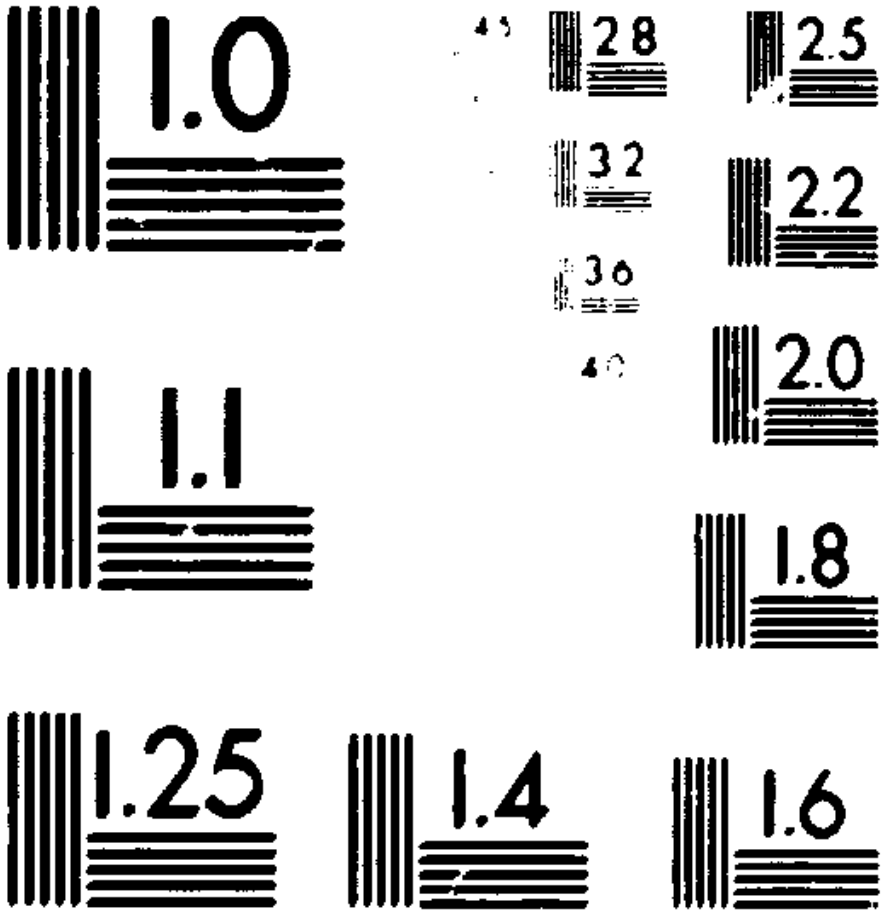

5. CELL VOLTAGE AND ENERGY BALANCE ON ALUMINIUM REDUCTION CELLS

5.1 Theoretical energy requirement of Hall-Hercult process

Electrical energy required electrolysis for the aluminium production by is equal to the change in Gibbs free energy of cell reaction.

The relation between the Gibbs free energy and reversible cell voltage is:

$$\Delta G = -nFE_r \qquad (5.1)$$

In total energy requirement, however, is:

$$\Delta H = \Delta G + T\Delta S \qquad (5.2)$$

It means, that the cell would be cooled, if heat is not supplied externally.

At 1000 ^{o}C the Gibbs-function for aluminium producing reaction 640 KJ/mole. The total energy requirement ΔH is larger than ΔG, around 845 KJ/mole. If the reaction takes place reversibily, and G is the energy quantity put into the system, the balance, $T\Delta S$, would have to be taken from the system's heat content.

For the primary cell reaction, the entalphy is about 550 KJ/mole at 1000 ^{o}C. The theoretical energy requirement to produce 1 kg Al at this temperature 5.64 kWh/kg Al, as compared with 8.69 kWh/kg Al for the decomposition of

oxide without carbon as reducing agent. So, electrical energy is saved at the expence of carbon consumption.

The earlier was discussed, that the loss in current efficiency (CE) due to the reoxidation process.

$$\frac{1}{2}Al_2O_3 + \frac{3}{4x}\,C = Al + \frac{3}{4}\,(2-\frac{1}{x})\,CO_2 + \frac{3}{2}\,(\frac{1}{x}-1)\,CO \qquad (5.3)$$

X - means the current efficiency.

To obtain the correct expression for the energy requirement for the real process, taking the reduced current efficiency into account.

The enthalpy requirement per mol aluminium is

$$\Delta H_{tot} = \Delta H_{reac,T} + \frac{1}{2}\,(H_T^{\circ} - H_{298})_{Al_2O_3} + \frac{3}{4x}\,(H_T - H_{298})C$$

$$= \Delta H_{reac,\,298} + (H_{933} - H_{298})_{Al_s} + \Delta H_{fus,Al} +$$

$$(H_T^{\circ} - H_{933}^{\circ})_{Al(l)} + \frac{3}{4}\,(2-\frac{1}{x})\,(H_T - H_{298})CO_{2g} +$$

$$\frac{3}{2}(\frac{1}{x}-1)\,(H_T - H_{298})_{CO(g)} \qquad (5.4)$$

The various energy terms calculated as function of current efficiency are

$$\Delta H_t = \frac{139.180}{X} + 477.240 \text{ KJ mol}^{-1} \text{ Al} \qquad (5.5)$$

$$= \frac{1.43}{X} + 4.91 \text{ kWh kg}^{-1} \text{ Al} \quad \text{(See Ref.65.} \qquad (5.6)$$

This value gives the total minimum energy requirement as a function of the current efficiency.

The specific electrical energy consumption is given by the relationship

$$\text{kWh/kg Al} = 2.98 \quad \frac{E_{cell}}{\%CE} \tag{5.7}$$

where E_{cell} is total cell voltage.

It is obvious from this relationship that only cell voltage and current efficiency determine electric power consumption. Factors governing current efficiency is discussed in the previous chapter. Now the factors governing cell voltage is examined.

5.2 Cell voltage components

Cell voltage can be broken down into components

$$E_{cell} = E^{o} + \eta_{rA} + \eta_{CA} + \eta_{CC} - I\,(R_A+R_S+R_C+R_X) \tag{5.8}$$

Using the thermodynamic sign connection considers energy production positive and energy consumption negative.

E^{o} is the thermodynamic equilibrium potential for primary reaction:
E^{o} is calculated by Nernst-equation

$$E^{o} = -\frac{\Delta G}{nF} + \frac{RT}{6F} \ln \frac{a_{Al}^{2}\, a_{CO_2}^{1.5}}{a_{Al_2O_3} \cdot a_{C}^{1.5}} \tag{5.9}$$

where: ΔG = the free energy change for the primary reaction.

The activities $a_{Al} = 1$ $a_C = 1$ and $a_{CO_2} = 1$

The alumina is in solution, however, and will have unit activity only at saturation. It is possible determination of activity of alumina.

Method and its problema was described in Chapter 2.

Activity of alumina is measured by Vetjukov and Rolim, expecting these data can be calculated the alumina activity at other concentrations (6, 7).

$$a_{Al_2O_3} = \left(\frac{\%Al_2O_3}{\%Al_2O_3 \text{ sat}} \right)^{2.77} \qquad (5.10)$$

On this basis E^o will be -1.207 volts at 1243^oK.

The next terms are the reaction and concentration overvoltage at the anode. (In Chapter 2 was discussed)

The η_{CC} means the concentration overvoltage at the cathode. In Chapter 2 was discussed.

The summation of $E^o + \eta_{RA} + \eta_{CA} + \eta_{CC}$ terms given the CEMF (counter electromotive Force) of the cell or voltage, that would be observed if the current is momentary interrupted.

The remaining terms are ohmic. Total cell current is represented by I. R_A represents the ohmic resistance of the anode and its attachment for conducting electrical current into the anode. Likewise, R_C represents the ohmic resistance of the cathode assembly. It consists of the metal pad, carbon lining, and collector bar extending into the lining. R_x represents the ohmic resistance of the bus bars external to the cell.

The ohmic resistance of the electrolyte is represented by R_B. The electrical conductivity of the electrolyte is influenced not only by composition and temperature but also by gas bubbles. Carbon dust affects electrical conductivity similarly to gas bubbles.

The total ohmic resistance of the electrolyte is

$$R_B = R_{Bu} + R_{Ba} \qquad (5.11)$$

R_{Bu} - bath resistance uncorrected for bubbles adhering to anode

R_{Ba} - added resistance caused by bubbles adhesing to the anode.

Cell voltage components are shown is and its relationship with energy consumption, in Fig.43. (64)

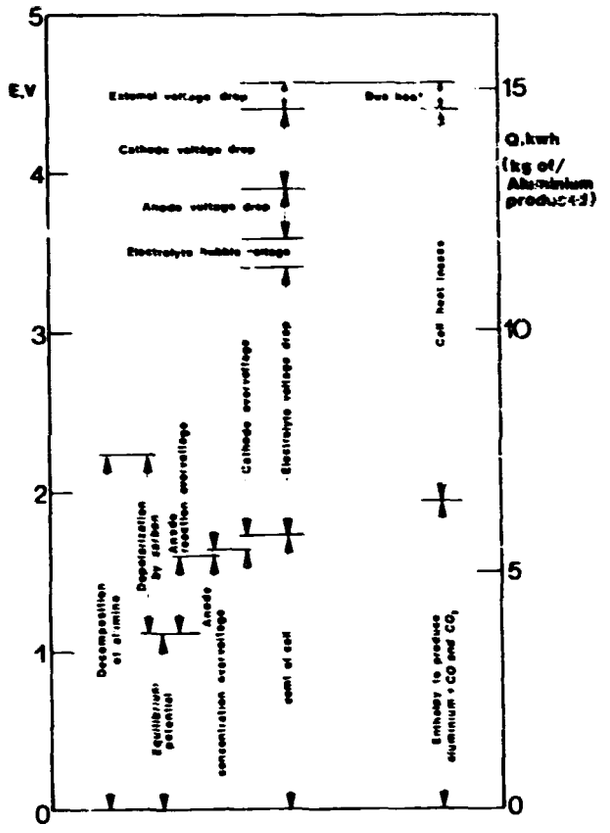

Cell voltage and current efficiency determine the kWh/kg of Al produced. There is no assurance, however, that the cell will have a satisfactory heat balance. The steady-state energy balance is.

$$E \cdot I = E_{(Al)} \quad I + Q \tag{5.12}$$

I - cell line

Q - rate of heat loss

$$E_{Al} = - \frac{\Delta H_R}{6F} \quad \frac{\%CE}{100} \tag{5.13}$$

Very important is to calculate the heat losses. If they equal the calculated heat loss available, the cell satisfies the heat balance requirement.

Briefly, powerful computers make it possible to matematically model the steady state condition within a Hall-Heroult cell with good occuracy. Such modeling helps to predict conditions to conserve energy.

5.3 Energy efficiency

The Hall-Heroult process for aluminium production has the disadvantage of rather low energy efficiency EE. Since the enthalpy of the overall process is more positive than the Gibbs free energy, the energy efficiency should be defined as the sum of enthalpy of reaction plus the energy needed to heat the raw materials divided by energy input to the cell

$$EE = \frac{\Delta H_T + H_{T_{298}}}{E_{input}} = \frac{\Delta H_T + H_{T_{298}}}{\frac{1}{x} \cdot nFE_{cell}} \qquad (5.14)$$

$$EE = \frac{X \quad H_{reac\ T} + \frac{1}{2}\,(H_T - H_{298})_{Al_2O_3} + \frac{3}{4x}\,(H_T - H_{298})y}{nFE_{cell}} \qquad (5.15)$$

$$EE = \frac{0.481 + 1.65x}{E_{cell}} \qquad (5.16)$$

Inserting avarage values for current efficiency 90 % and for the cell voltage 4.5 V gives an energy efficiency not more than 43.7 %. (65)

The cell voltage is much higher value than the reversible cell voltage. Consequently only about one fourth of energy input, E_{input} is expended to cover the electrical work (ΔG).

The difference between the cell voltage and the reversible cell voltage is due to.

- anodic overvoltage (0.5-0.6 V)
- voltage drop in bath
- voltage drop in anodic part
- voltage drop in cathodic part
- voltage drop in the electrical connections
- an average increase caused by the anode effect.

The energy balance is:

$$E_{input} = \Delta G + E_{ohmic} = \Delta H - T\Delta S + E_{ohmic} \qquad (5.17)$$

where E_{ohmic} is the ohmic heat developed.

The energy difference has to be disposed of the heat.

$$E_{input} - \Delta H_{tot} = E_{ohmic} - T\Delta S = Q \qquad (5.18)$$

The low value of the EE can be improved by either increasing the current efficiency of decreasing the cell voltage.

6. FUTURE TRENDS, RESEARCH AND DEVELOPING PROGRAMS IN PROCESS METALLURGY OF ALUMINIUM

Twenty years ago the most aluminium electrolysis cells were operated at 70.000 A, but nowadays the cells accomodate currents up about 280 000 A. These cells have the potential for incrased energy efficiency. (66)

The large cells show cost savings, because most operating expenses in a aluminium smelting plant are related to the number of cell.

Because of rising cost of energy the new cells are designed for lower current density. The last two decades the decrease in energy requirement was from 17 to 13 kWh/kg. But since the theoretical limit at 970 ^{o}C is 6.34 kWh/kg Al, there is obviously still opportunity for energy saving.

Improvement in Hall-Heroult energy efficiency has come from increased anode area. From a given cell amperage the larger anode area maintains lower current density and voltage. Cell design has provided the option of lower density in order to achive lower voltage. The lower current density cells must be larger and hence more costly and they require additional heat insulation.

Another area of improvement in Hall-Heroult operation means the removal of fluoride fume from cell off gas. Fluoride is sorbed onto the alumina which then fed to the cells. Aluminium fluoride consumption has been decreased significantly.

Aluminium fluoride additions also the lower the melting point of the electrolyte, permitting lower operating temperature Hence adding aluminium fluoride can increase current efficiency. Aluminium fluoride additions increase fluoride evolution and decrease electrical conductivity. At the lower operating temperatures, the alumina solubility and rate of solution are decreased. This can lead to sludge formation on the bottom of cell. To avoid the sludge formation the average alumina content in the electrolyte is 2-3.5 wt%.

It is necessary to have frozen bath covering the outer periphery of the cell bottom to minimize metal pad disturbances from horizontal current flow. Little insulation on the bottom leads to excessive frozen bath which covers the cathode, increasing voltage and interfering with circulation.

Excessive insulation will prevent freezing of the bath and this results in erosion and early lining failure.

The techniques for calculating heat losses have been improved by matematical modell.

The heat flow instruments are available to optimize the insulation. These instruments permit determination of points of lining failure when bath penetrates into pot insulation.

In future the existing Hall-Heroult cells will continue to operate.

There are different R & D projects in experimental stages:

Inert anode, the most obvious advantage of inert anodes is saving of carbon and the possibility of a fixed anode with constant interpolar distance. The idea of a chemically inert anode is attractive, because it offers possibilities of a more compact cell design. (67)

Bipolar cell arrangements with biplar electrode of inert anode material in combination with a cathode material of graphite or TiB_2 have been suggested. The advantage of such a cell arrangement would be shorter anode-cathode distance, reduced ohmic resistance and reduced heat losses. This means compact cell design and high production capacity per unit.

REFERENCES

1.) Grjotheim, K., et Al., "Aluminium Electrolysis", Aluminum-Verlag Gmbh, Dusseldorf, 1977.

2.) The Interna ional Course on Process Metallurgy of Aluminium, Trondheim, Norvay

3.) Yim E, W. and Feinleib, M.: J. Electrochem. Soc. 104, 626 (1957)

4.) Thonstad, J. and Rolseth, S: Proceedings 3rd ICSOBA Conference, Nice, Sept. 1973. p.657

5.) Thonstad, J.: Electrochim acta 15. 1569 (1970)

6.) Vetyukov, M.M. and Van Ban, N.: Tsvet. Met. 44 (8) 31 (1971) Sov. J. Non Ferrous

7.) Rolin, M. and Gallay, J.J: Electrochmica Acta 7. 153. (1962)

8.) Haupin, W.E.: J. Metals 23, (10) 46 (1971)

9.) Thonstad, J.: Electrochem. Techn. 6 346 (19

10.) Dewing, E.W: Met. Trans., 1 2211 (1970)

11.) Horvath, J: 4th Conference of the Socialist Countries on Molten Salt Chemistry and Electrochemistry Balatonfüred, Hungary 1981. Extended Abstracts.

12.) Calandra, A.J., Castellano, C.E., Ferro, C.M., and Cobo, O.; Light Metals 1982, p.345, Metallurgical Soc. of AIME

13.) Thonstad, J.: Electrochim Acta 1967 12, 1219

14) Piontelli, R., Mazza, B. and Pedefferi, P.: Metallurgica Ital. 1965 57 (2), 1, 51.

15.) Thonstad, J., Solbu, A. and Larsen, A.: J. Applied Electrochem. 1. 261. (1971)

16.) Horváth, J., Pőcze, I., Zaymus, M.: 4th Conference of the Socialist Countries on Molten Salt Chemistry and Electrochemistry Balatonfüred, Hungary, 1981. Extended Abstracts.

17.) Pőcze, I., Tikasz, L., Zaymus, M: ALUTERV-FKI, Internal Study 1982.

18.) Borisoglebski, Y.V., Vetyukov, M.M., and Vinohurov, V.S.: Tsvet. Met. 44 (10), 37 (1971)

19.) Raj, N.P., Várhegyi, G., and Horváth, I.: Kohászati Lapok 112, 475 (1979)

20.) Thonstad, I. and Rolseth, S.: Electrochim, Acta 23 (223) (1978)

21.) Koratov, M.A. and Chanlytek, V.I.: Sov. J. Non-Ferrous Met. 14 (3) (32)

22.) Revazyan, A.A., Grigoryan, B.S.: Arm. Khim Zk. 26 (1) 65 (1973)

23.) Revazyan, A.A.: Tsvet. Met. 33 (3) 51 (1960)

24.) Balázs, E., and Mosóczi, F.: Intern. Symp. of ICSOBA, Budapest 1969 vol.IV.

25.) Mosóczi, F. Kohászati Lapok 109, 7-8, (1976)

26.) Borsimenko, O.P., Vetyukov, M.M: Zh.Prike. Khim. 8. 1969 (1966)

27.) Haupin, W.E. and McGrew, W.C.: Aluminium 51, 273 (1975)

28.) Kvande, H.: Dr.tech. Thesis NTH, The University of Trondheim, Norway 1979

29.) M.Szakszon, E.Berecz, J. Horváth, G. Szina,: Proceedings of the 4th Conference on Applied Chemistry Unit Operations and Processes Vol.2. 145 (1983) Veszprém (Hungary)

30.) I. Ubrankovics, I. Horváth, G. Szina, P.Káldi, Proceedings of the 4th Comference an Applied Chemistry Unit Operations and Processes Vol.2. 134. (1983) Veszprém (Hungary)

31.) Thonstad, J. Light Metals 1981. Metallurgical Cos. of AIME

32.) S.Gjertad and B.J.Welch.: J. Electrochem. Soc., 111 (8) (1964)

33.) Yu.I. Dvinin: Sov.J. Non-Ferrous Met. 11 (4) 1970, p.49.

34.) A.M. Arthur: Met. Trans., 5 (1974) pp. 1225-1229

35.) Research Report on determination of aluminium inventory in operating aluminium cells ALUTERV-FKI, 1982.

36.) Beck, T.R.: J.Electrochem. Soc. 106, 710 (1959)

37.) Hamlin, J.D. and Richards, N.E.: in Extractive Metallurgy of Aluminium, Vol.2. Interscience Publishers, New York, 1963 p.51

38.) Q. Zhuxian and F. Naixiang: Aluminium 59. (1983)

39.) Abramov, G.A., Vetyukov, M.M.: Theoretical Principles of the Electrometallurgy of Aluminium Metallurgizdat, Moscow 1953

40.) Thonstad, J., and Liu, Ye: Light Metals 1981, Proceedings of sessions 110th AIME Annual Meeting, Chicago

41.) Gjerstad, S. and Richards N.E: Paper presented at Symposium, Electrochem. Soc., Cleveland, 1966

42.) Schlain, D., and Swift, J.H.: USA Bureau of Mines, Report 1963.

43.) Poole, R.T. and Etheridge, C.: Light Metals 1977. Atlanta, Proceedings of sessions 106th AIME Annual Meeting

44.) Saakyan, P.S.: Zh. Prikl. Khim. 39, 357 (1966)

45.) Thonstad, J., J. Electrochem. Soc. 111 959 (1964)

46.) Mc Minn, C.J., "Current Efficiency in 2500 A Reduction Cells". Reference Report, Reynolds Met. Comp. Alabama (1958)

47.) Balåzs, E. and Belyaev A.I., Izv. vyssh. uchebn. Zav. Tsvetn. Met. 4 (3) 67 (1961)

48.) Schmitt, H. Extractive Metallurgy of Aluminium Vol.2. Interscience Publishers (1963)

49.) Grjotheim, K., Malinovszky, M., Thonstad, J., Can.Met. Quart. 11 (2) 295 (1972)

50.) Forsblam, G.V. and Sandler, R.A., Tsvetn. Met. 29 (6) 47

51.) Ferber, M., Alluminio 9 (453) (1965)

52.) Fellner, P., Grjotheim, K., Matiasovsky, K. and Thonstad, J., Can. Met. Quart. 8 245 (1969)

53.) Wieugel, J. and Bøckman, O.C., J. Electrochem. Soc. 101 145c (1954)

54.) Molnar, I., The 2nd International Conference of the ICSOBA, Budapest (1969)

55.) Schmitt, H., In "Extractive Metallurgy of Aluminium", Vol. 2, (Edited by Gerard, G.), Interscience Publishers, New York (1963)

56.) Pruvot, E., Alluminio 22 721 (1953)

57.) Thonstad, J., Nordmo, F. and Paulsen, J.B.,: Metallurgical Transactions, Vol. 3, February 1972, pp. 403-407.

58.) O.A. Asbjørnsen, J.A. Andersen,: Light Metals 1977 Volume 1. Proceedings of Sessions 106th AIME Annual Meeting Atlanta, Georgia

59.) J.Thonstad, W.Kristensen, Light Metals 1958

60.) R.K. Jain, S.B. Tricklebank and B.J.Welch, D.J. Williams: Light Metals 1982

61.) K.Grjotheim, R.Naeumann, H.A.Oye: Light Metals 1977 Volume 1.

62.) Grjotheim, K., Jørgensen, S., Nikolic, R. and Øye, H.A., Metall 30 (1976) 546.

63.) Belitskus, D.: Light Metals, 1976, Vol. 1, Proceedings of Sessions, 105th AIME Annual Meeting, Las Vegas, Nevada, 1976, p.411.

64.) V.E.Haupen and W.F.Frank: Electrometallurgy of Aluminium

65.) D.Bratland, K.Grjotheim, C.Krohn: Light Metals 1976, Volume 1, Proceedings of Sessions 105th AIME Annual Meeting Las Vegas, Nevada

66.) E.Russell: International course the process metallurgy of aluminium. Norway Trondheim 1983.

67.) Billehaug,K. and Øye, H.A.: Aluminium 57, 146 and 228)1981)